NO adsorption and thermal behavior on Pd surfaces. A detailed comparative study

R.D. Ramsier [a], Q. Gao [a], H. Neergaard Waltenburg [a], K.-W. Lee [a], O.W. Nooij [b], L. Lefferts [a], J.T. Yates, Jr. [a],*

[a] *Department of Chemistry, University of Pittsburgh, Surface Science Center, Pittsburgh, PA 15260, USA*
[b] *Department of Physics, Eindhoven University of Technology, Eindhoven, Netherlands*

Abstract

The adsorption and thermal behavior of NO on 'flat' Pd(111) and 'stepped' Pd(112) surfaces has been investigated by temperature programmed desorption (TPD), high resolution electron energy loss spectroscopy (HREELS), and electron stimulated desorption ion angular distribution (ESDIAD) techniques. NO is shown to molecularly adsorb on both Pd(111) and Pd(112) in the temperature range 100–373 K. NO thermally desorbs predominantly molecularly from Pd(111) near 500 K with an activation energy and pre-exponential factor of desorption which strongly depend on the initial NO surface coverage. In contrast, NO decomposes substantially on Pd(112) upon heating, with relatively large amounts of N_2 and N_2O desorbing near 500 K, in addition to NO. The fractional amount of NO dissociation on Pd(112) during heating is observed to be a strong function of the initial NO surface coverage. HREELS results indicate that the thermal dissociation of NO on both Pd(111) and Pd(112) occurs upon annealing to 490 K, forming surface-bound O on both surfaces. Evidence for the formation of sub-surface O via NO thermal dissociation is found only on Pd(112), and is verified by dissociative O_2 adsorption experiments. Both surface-bound O and sub-surface O dissolve into the Pd bulk upon annealing of both surfaces to 550 K. HREELS and ESDIAD data consistently indicate that NO preferentially adsorbs on the (111) terrace sites of Pd(112) at low coverages, filling the (001) step sites only at high coverage. This result was verified for adsorption temperatures in the range 100–373 K. In addition, the thermal dissociation of NO on Pd(112) is most prevalent at low coverages, where only terrace sites are occupied by NO. Thus, by direct comparison to NO/Pd(111), this study shows that the presence of steps on the Pd(112) surface enhances the thermal dissociation of NO, but that adsorption at the step sites is not the criterion for this decomposition.

1. Introduction

A fundamentally important question in surface science which has yet to be answered in general is: What is the role of surface structure in controlling the surface chemistry of adsorbed molecules? This question was conceptually raised in the early writings of Taylor [1], who envisioned that there were certain sites on a solid surface which were preferentially involved in the thermal reactions of adsorbed species. Although a great deal of understanding about the details of surface chemistry has been developed in recent decades [2], it is still not possible to provide a general answer to the question posed above. To investigate this topic in detail, one can choose a

---

* Corresponding author. Fax: +1 412 624 6003.

specific adsorbate/substrate system and systematically vary the substrate surface structure, exposing the reactant molecule to different substrate crystal planes. This permits the extraction of detailed information regarding the role that surface structure plays in controlling chemical reactions.

Along these lines, the present study focuses on the behavior of nitric oxide (NO) adsorbed on two related Pd single crystal surfaces. It will be shown that NO adsorption ($100 \leqslant T_{ads} \leqslant 373$ K) on the 'flat' Pd(111) surface is molecular, with the N–O bond axis oriented along the $\langle 111 \rangle$ surface normal, independent of surface coverage. Upon heating, NO reversibly desorbs from Pd(111) with minimal decomposition, exhibiting first-order desorption kinetics with a desorption activation energy and pre-exponential factor which strongly depend on the initial NO surface coverage. A slight amount of NO thermal dissociation upon heating to ~ 490 K deposits small amounts of surface-bound O on Pd(111), which dissolves into the Pd bulk upon heating above 550 K.

NO adsorption ($100 \leqslant T_{ads} \leqslant 373$ K) on the 'stepped' Pd(112) surface (Pd(S)[3(111) × (001)]) will also be shown to be molecular. However, contrary to the behavior observed in other systems, NO preferentially adsorbs at low coverages on the (111) *terrace sites* of Pd(112). Only at high coverages are both terrace and step sites occupied by NO on Pd(112). Upon heating, N_2 and N_2O, in addition to NO, desorb from NO/Pd(112) in much larger relative yields than observed for NO/Pd(111). This result indicates that the thermal decomposition of NO on the stepped surface competes more successfully with NO thermal desorption, as compared to the flat surface. The fractional amount of NO dissociation on Pd(112) upon heating is largest at the lowest NO coverages, where only terrace sites are occupied by NO. Evidence will be presented for the formation of both surface-bound O and sub-surface O on Pd(112) following the thermal decomposition of NO. This oxygen diffuses into the Pd bulk at temperatures above 550 K.

2. Experimental

Both of the stainless steel ultra-high vacuum (UHV) systems employed in this study operated at base pressures of $< 1 \times 10^{-10}$ Torr. The first UHV chamber contained an ion sputtering gun, a flux calibrated microcapillary array beam doser [3–5], a cylindrical mirror analyzer (CMA) for Auger electron spectroscopy (AES), a quadrupole mass spectrometer (QMS) for temperature programmed desorption (TPD), and a combination low energy electron diffraction (LEED) and electron stimulated desorption ion angular distribution (ESDIAD) apparatus [6,7]. In addition, a second electron gun mounted in this system could be used to induce electron stimulated desorption (ESD) of positive ions from the NO-covered Pd surfaces, with transmission into the QMS (ionizer turned off) for mass identification.

All of the TPD data presented in this report were recorded in the first UHV chamber. The QMS ionizing energy was 70 eV, and a -150 V bias was applied to the crystal during TPD to prevent possible ESD damage to adsorbed NO by stray electrons from the QMS. The heating rates employed for TPD were 4.0 K/s (NO/Pd(111)) and 2.0 K/s (NO/Pd(112)), with temperatures measured via a chromel–alumel thermocouple spot welded to the edge of the crystal.

The ESDIAD patterns presented in this work were acquired at 100 K in the first vacuum system with incident electron beam energies (E_i) in the 800–1000 eV range. The electron beam currents ($I \approx 5$ nA) were measured between the crystal and ground and are uncorrected for secondary electron yield. These small currents were deliberately chosen to minimize the ESD damage ($< 1\%$, see the Appendix) to adsorbed NO and to avoid raising the crystal temperature significantly (< 1 K) during ESDIAD data acquisition. The ESDIAD data were acquired under field-free conditions, with the crystal and the first grid of the detection optics grounded. The ESDIAD patterns were digitally stored as a 64 × 64 array and were processed by digital smoothing and subtraction of a large X-ray background signal [6,7].

The second UHV chamber housed an ion sputtering gun, a flux calibrated microcapillary array beam doser [3–5], a CMA for AES, a QMS for TPD, LEED optics, and a high resolution electron energy loss spectrometer (HREELS). The HREELS data presented in this study was acquired at 100 K. The primary beam energy utilized for HREELS was $\sim$ 4.5 eV and the full width at half maximum of the elastic peak was about 60 cm^{-1}. Typical counting

rates of 1×10^5 counts per second were measured for the HREELS elastic beam from the clean Pd surfaces, and the HREELS data have been digitally smoothed [8].

Both the Pd(111) and Pd(112) single crystals employed in this study were cut from the same high-purity boule, which was cylindrical in shape with a diameter ~ 0.93 cm. The crystal surfaces were mechanically polished to mirror finish and oriented within 0.5° using Laue X-ray diffraction. Once under UHV conditions, the Pd surfaces were cleaned by 1000 K Ar^+ ion sputtering ($E_i = 2$ keV, $I = 2\mu A$) in the presence of $\sim 4 \times 10^{-8}$ Torr of O_2. This was followed by 1000 K annealing in $\sim 2 \times 10^{-7}$ Torr O_2 and then flash annealing to 1200 K in vacuum before measurements were performed. This cleaning procedure was repeated, in whole or in part, until AES showed no evidence for the impurities S (< 0.1 at%), O (< 0.5 at%), and C [9–13]. Due to overlapping C(KLL) and Pd(MNN) AES features [9–13], the final test of surface cleanliness was the lack (< 0.01 monolayer (ML)) of CO and CO_2 thermal desorption from the Pd surfaces following adsorption of oxygen at room temperature. LEED was then employed to verify the proper structure of the clean Pd surfaces.

Nitric oxide ([14]NO, Matheson, 99% pure) and [15]NO (Cambridge Isotopes, 99% isotopically pure) was transferred into individual glass bulbs attached to the gas-handling systems. Freeze–pump–thaw cycles were employed for purification, and pure white crystalline NO was observed in the storage bulbs at liquid nitrogen temperature. Line-of-sight dosing into the QMS was used to verify the purity of these gases. NO was introduced onto the crystals with flux calibrated beam dosers [3–5] housed in both vacuum chambers; uncertainties in the cross-calibration of the two dosers are within 10%.

3. Results

3.1. Temperature programmed desorption

All of the TPD data presented here were acquired in the same UHV system following 300 K adsorption of NO on clean Pd(111) and Pd(112) surfaces. Isotopically labelled [15]NO was employed for TPD (al-

though not shown here for Pd(111)) in order that the observed products of [15]NO dissociation ([15]N_2, 30 amu and [15]N_2O, 46 amu) could be clearly distinguished from CO (28 amu) and CO_2 (44 amu). These carbon-containing species were undetectable (< 0.01 ML) during TPD of [15]NO from either clean Pd surface. Additionally, no desorption of O_2 or NO_2 was observed by TPD under any conditions from [14]NO or [15]NO adsorbed on either Pd(111) or Pd(112).

The 'relative yields' to be discussed are the ratios of the integrated TPD areas of the observed NO decomposition products, [15]N_2 and [15]N_2O, to the corresponding area of the [15]NO TPD spectrum acquired simultaneously by multiplexing the QMS. The integrated areas of the TPD spectra are reproducible to within 5%, and the uncertainty in the relative yields is therefore considered to be $\pm 11\%$. No corrections to the TPD areas (and therefore to the
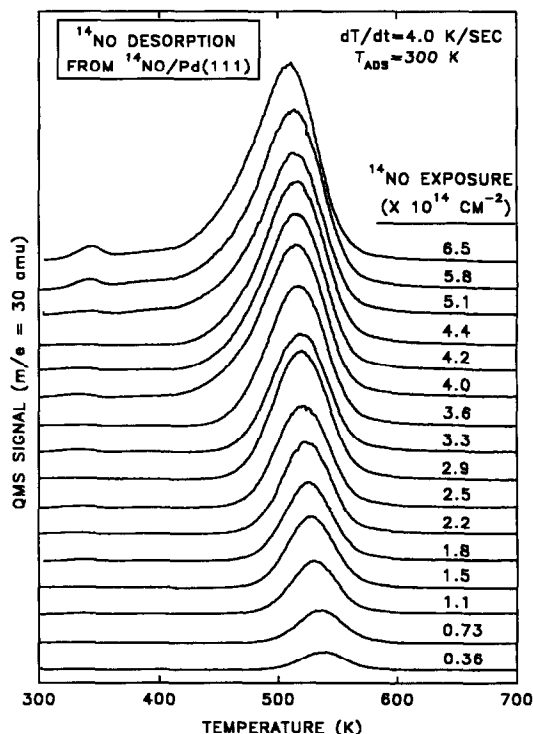

Fig. 1. Temperature programmed desorption spectra of [14]NO ($m/e = 30$ amu) following adsorption of various amounts of [14]NO on Pd(111) at 300 K. A heating rate of 4.0 K/s was employed.

relative yields) have been made for the different desorbing molecules due to variations in ionization probability, QMS throughput efficiency, QMS multiplier gain, chamber wall effects or chamber pumping speeds. The uncertainties associated with each of these factors makes such corrections questionable. Therefore, the relative yields of NO dissociation products observed during TPD are used comparatively for the two Pd crystals, and are not discussed in terms of absolute amounts of these species.

3.1.1. NO / Pd(111)

Fig. 1 presents TPD spectra of ^{14}NO (30 amu) from ^{14}NO/Pd(111). Under all conditions tested, a relative yield < 0.005 for the desorption of N_2O was observed following 300 K adsorption of ^{14}NO or ^{15}NO on Pd(111) [14]. However, N_2 thermal desorption was observed by TPD to approximately coincide with that of NO, with a small relative yield of 0.017 at high NO coverages [14]. These results indicate that only a very slight amount of NO dissociation
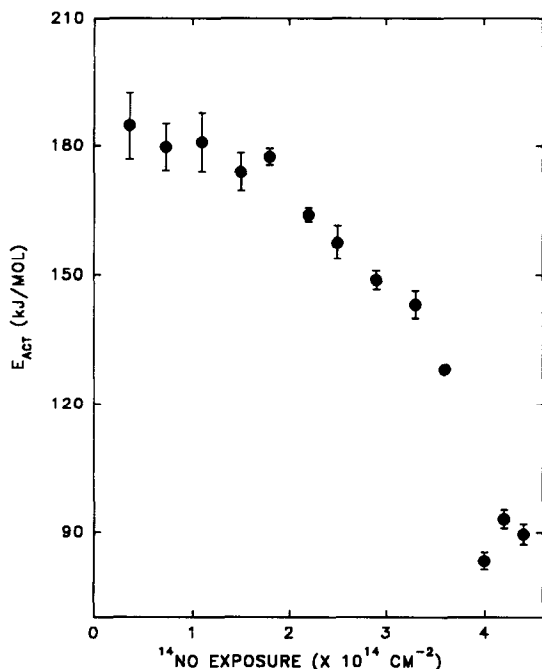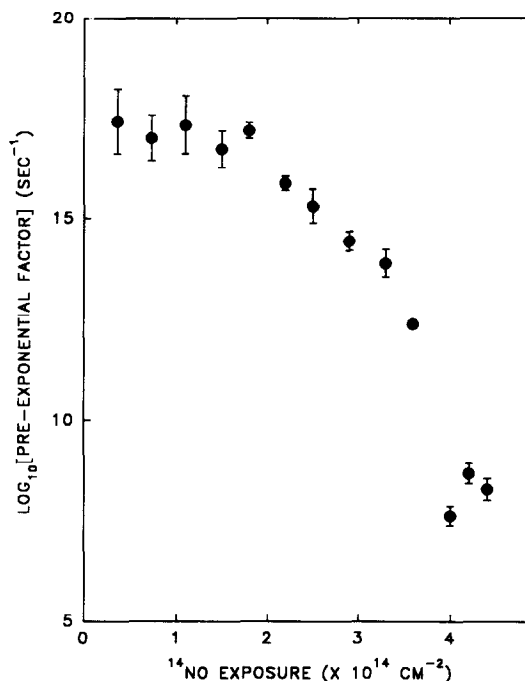

Fig. 3. Logarithmic plot of the pre-exponential factor of desorption of ^{14}NO from Pd(111) calculated from the desorption spectra of Fig. 1. This data closely mirrors that shown for E_{act} in Fig. 2, due to the 'compensation effect' often found in laterally interacting systems (see text).

occurs on Pd(111) during heating, possibly due to the presence of a small surface defect density.

It is seen in Fig. 1 that the thermal desorption of NO from Pd(111) occurs near 540 K at low coverage, shifting to near 510 K at higher coverages. The first-order kinetic parameters (activation energy of desorption, E_{act}, and pre-exponential factor) of NO thermal desorption from Pd(111) have been calculated from the data of Fig. 1, and are shown in Figs. 2 and 3, respectively. The calculations were performed following the threshold temperature programmed desorption (TTPD) method [15], which relies on detailed analysis of the leading edge of a thermal desorption feature at various coverages. Figs. 2 and 3 resulted from such analysis of the first 5% (integrated area) of the lower 13 spectra of Fig. 1. Above an NO exposure of 4.4×10^{14} cm^{-2}, low temperature NO desorption features (300–400 K) interfered with the linear background needed for TTPD analysis.

Fig. 2. The activation energy of first-order desorption of ^{14}NO from Pd(111) calculated from the spectra of Fig. 1 using the threshold temperature programmed desorption method. The decrease in E_{act} as the ^{14}NO exposure increases indicates the presence of repulsive interactions between the adsorbed species.

As is evident in Figs. 2 and 3, both the activation energy and pre-exponential factor of NO thermal desorption from Pd(111) are strongly dependent on initial NO coverage. Both kinetic parameters have seemingly high values ($\sim$ 180 kJ/mol and $\sim 10^{17}$ s^{-1}, respectively) at very low initial NO coverages, falling to $\sim$ 90 kJ/mol and $\sim 10^8$ s^{-1} at the highest coverages. The error bars of Figs. 2 and 3 indicate the uncertainty in a least-squares fit of a straight line to the Arrhenius plots derived from the data of Fig. 1 via the TTPD method [15].

3.1.2. NO / Pd(112)

Compared to NO/Pd(111), NO adsorbed on Pd(112) undergoes a significantly larger amount of decomposition upon heating [14]. TPD spectra acquired simultaneously following ^{15}NO adsorption on Pd(112) are shown in Fig. 4 (^{15}NO), Fig. 5 (^{15}N$_2$), and Fig. 6 (^{15}N$_2$O). The relative scales of Figs. 4–6 are indicated by the number of counts (an arbitrary unit) represented by a fixed height in each figure. As is evident from Figs. 4–6, the desorption yield of all
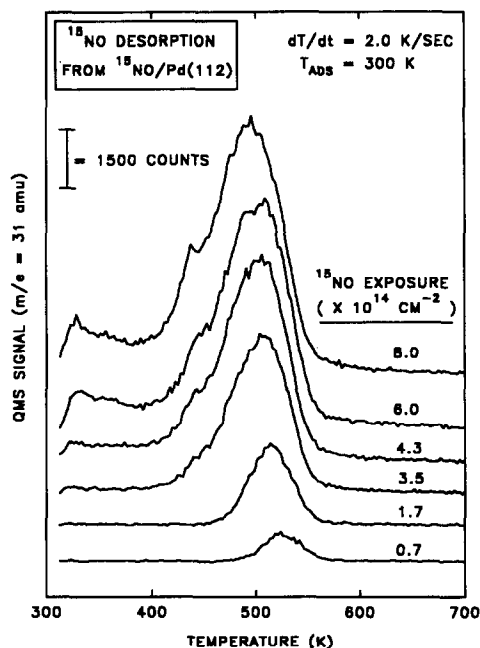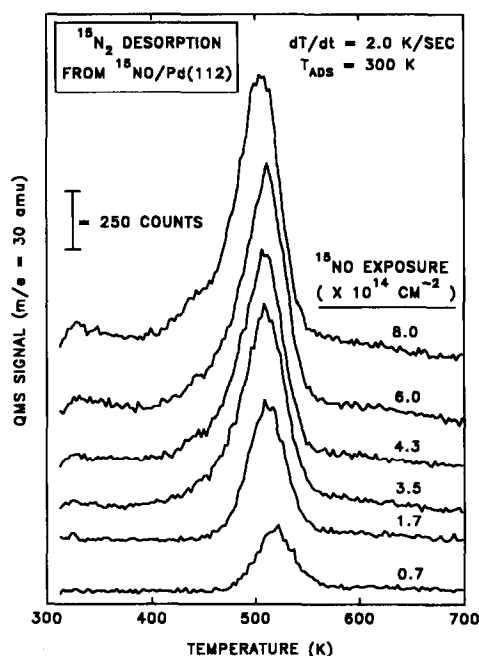

Fig. 5. Temperature programmed desorption spectra of ^{15}N$_2$ ($m/e = 30$ amu) following adsorption of various amounts of ^{15}NO on Pd(112) at 300 K. These spectra indicate that ^{15}NO dissociates substantially on Pd(112) upon heating, and that the amount of ^{15}N$_2$ produced by this thermal decomposition increases with ^{15}NO exposure. A heating rate of 2.0 K/s was employed.

three products increases monotonically with increased NO exposure, as determined by integration of the spectra [14].

The integrated areas of data like those of Figs. 4–6 have been used to calculate the relative TPD yields of ^{15}N$_2$ and ^{15}N$_2$O from ^{15}NO/Pd(112). As seen in Fig. 7, these relative yields are a strong function of NO coverage, with the largest fractional amount of NO decomposition occurring at the lowest NO exposures upon heating. Additionally, the relative yields of the products of NO dissociation (N$_2$ and N$_2$O) appear to saturate at the highest NO exposures in Fig. 7. The error bars of Fig. 7 represent the uncertainty in the relative yields discussed above ($\pm$ 11%), which are overshadowed by the size of the data points in some cases. No attempt has been made to analyze the TPD data from NO/Pd(112) for kinetic parameters of desorption, since Fig. 7 indicates that NO thermal decomposition competes with NO thermal desorption in varying degrees as the NO coverage is changed.

Fig. 4. Temperature programmed desorption spectra of ^{15}NO ($m/e = 31$ amu) following adsorption of various amounts of ^{15}NO on Pd(112) at 300 K. A heating rate of 2.0 K/s was employed.

3.2. High resolution electron energy loss spectroscopy

All of the HREEL spectra presented in this report were recorded at 100 K in the same UHV chamber following either 100 or 373 K adsorption of [14]NO on Pd(111) and Pd(112). NO exposures (not absolute NO surface coverages) are stated and should not be used to estimate relative coverages due to possible differences in the NO sticking coefficient between the two surfaces at different adsorption temperatures and coverages. Stepwise annealing experiments following NO adsorption employed a temperature ramp of 2.0 K/s to the desired temperature, followed by cooling to 100 K for HREELS data acquisition. During cooling and data acquisition, trace amounts (< 0.01 ML) of CO sometimes adsorbed on the Pd surfaces from the residual background gas of the UHV chamber. This adsorbed CO produces a vibrational feature near 1800 cm^{-1} in some of the HREEL

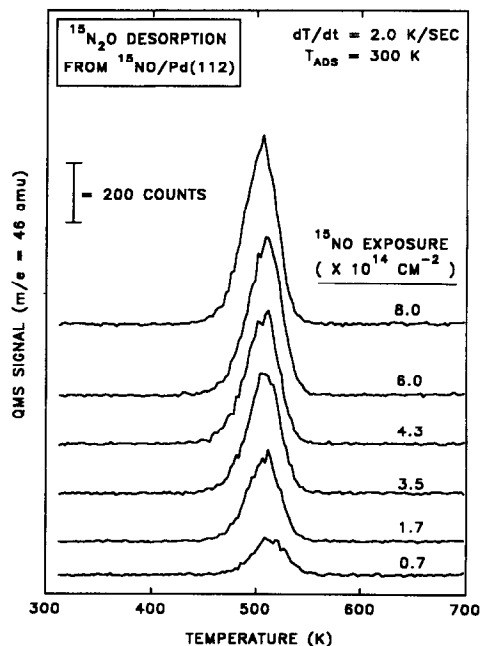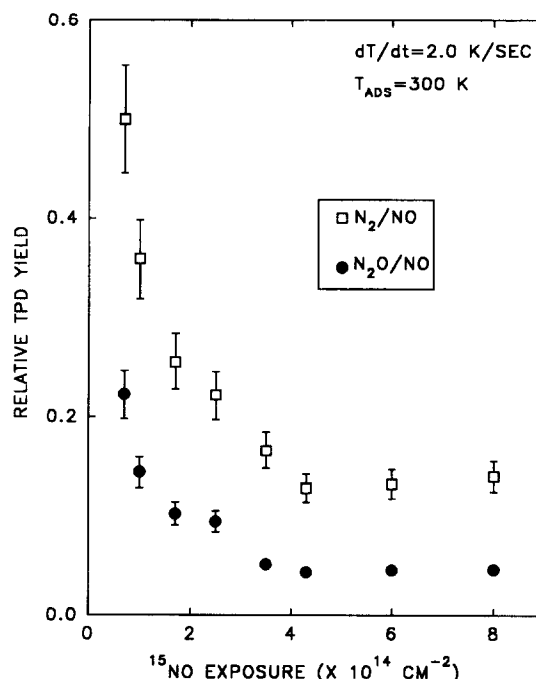Fig. 7. Relative yields ($\pm 11\%$) of the products of NO thermal dissociation on Pd(112) calculated from the integrated yields of spectra like those of Figs. 4–6. The fractional amount of NO dissociation is largest at low coverage and saturates at high coverage, indicating that lateral interactions between the adsorbed species play a major role in determining the thermal surface chemistry. Correction for the sensitivity of the mass spectrometer to the three desorption products has not been made.

spectra. This CO does not affect the interpretation of the results, as verified by controlled CO + NO coadsorption experiments.

3.2.1. 100 K adsorption: NO / Pd(111) and NO / Pd(112)

Fig. 8 presents HREELS data acquired following adsorption at 100 K of NO on Pd(111) at various NO exposures. The spectra indicate that NO adsorption is molecular on Pd(111) under these conditions. The N–O stretching mode (ν(N–O)) at 1535 cm^{-1} observed in the bottom spectrum of Fig. 8 shifts in frequency to 1600 cm^{-1} as the NO exposure is increased to 12×10^{14} cm^{-2}. At this NO exposure in Fig. 8, another ν(N–O) mode is observed at 1750 cm^{-1} (shoulder), which then increases in relative intensity as the NO exposure is raised further. The most important point in Fig. 8 is that NO adsorbed

Fig. 6. Temperature programmed desorption spectra of [15]N$_2$O ($m/e = 46$ amu) following adsorption of various amounts of [15]NO on Pd(112) at 300 K. These spectra indicate that [15]NO dissociates substantially on Pd(112) upon heating, and that the amount of [15]N$_2$O produced by this thermal decomposition increases with [15]NO exposure. A heating rate of 2.0 K/s was employed.

on Pd(111) at 100 K exhibits only two well-resolved ν(N–O) vibrational features at full coverage.

The HREEL spectra of Fig. 9 show that 100 K adsorption of NO on Pd(112) is also molecular. In the bottom spectrum of Fig. 9, a ν(N–O) mode at 1522 cm^{-1} is observed, with a small shoulder at ~ 1641 cm^{-1}. Increasing the NO exposure to 6.5 × 10^{14} cm^{-2} causes the lower frequency mode to shift to 1540 cm^{-1}, while the 1645 cm^{-1} ν(N–O) mode increases in relative intensity. Finally, at high NO exposures, ν(N–O) vibrational features at 1638 and 1738 cm^{-1} are seen in Fig. 9.

The most significant result of Fig. 9 is the presence of a ν(N–O) mode near 1645 cm^{-1} at intermediate NO coverages. This band is not observed by HREELS from NO/Pd(111) under similar conditions (Fig. 8), and the 1645 cm^{-1} mode is interpreted as resulting from NO adsorbed at the (001) step sites of Pd(112). The frequencies of the dominant vibrational modes from NO/Pd(111) and NO/

Fig. 9. High resolution electron energy loss spectra following adsorption of various amounts of NO on Pd(112) at 100 K. These spectra indicate that NO adsorption is molecular on Pd(112) under these conditions. By comparison with the low coverage spectra of Fig. 8, the 1522 cm^{-1} ν(N–O) band observed in the bottom spectrum is assigned to the vibrations of NO adsorbed at the (111) terrace sites of Pd(112). In addition, the 1645 cm^{-1} ν(N–O) mode observed here in the lower spectra, but not seen in Fig. 8 for Pd(111), is assigned to the vibrations of NO adsorbed at the (001) step sites of Pd(112).
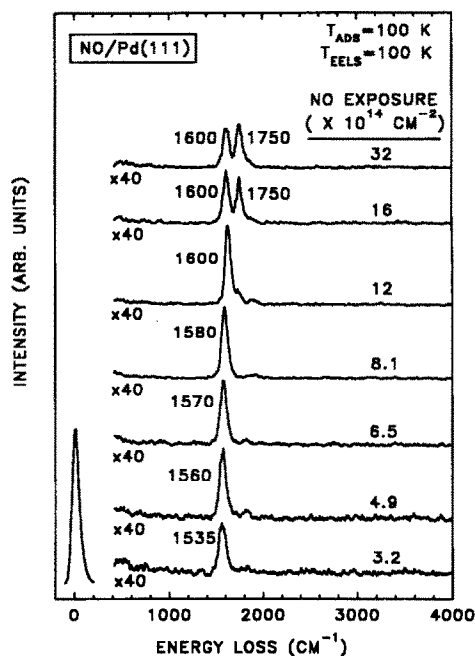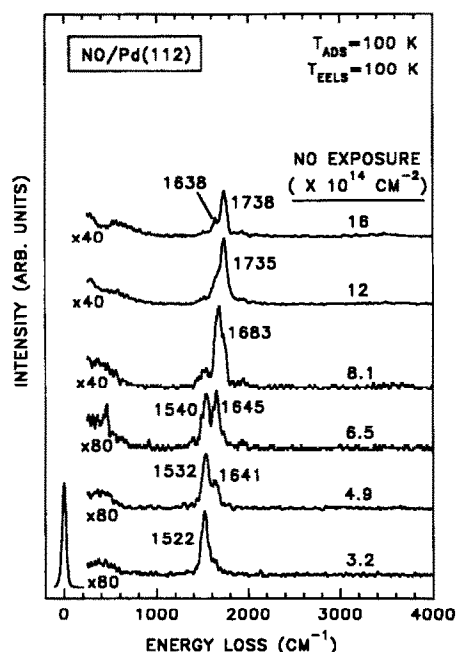

Fig. 8. High resolution electron energy loss spectra following adsorption of various amounts of NO on Pd(111) at 100 K. These spectra indicate that NO adsorption is molecular on Pd(111) under these conditions. Note that only two, well-resolved ν(N–O) modes are observed, shifting to higher frequency as the NO coverage is increased.

Pd(112) at the lowest NO exposures are strikingly similar (1535 and 1522 cm^{-1}) as shown in Figs. 8 and 9, respectively. These results indicate that at low coverages, NO preferentially adsorbs on the (111) terrace sites of Pd(112) at 100 K.

3.2.2. 373 K adsorption: NO /Pd(111) and NO /Pd(112)

The HREELS data of Fig. 10 were recorded following adsorption at 373 K of NO on Pd(111). As the exposure is increased, the ν(N–O) mode at 1540 cm^{-1} (bottom spectrum) shifts in frequency to 1590 cm^{-1}. This is the only ν(N–O) mode observed by HREELS for NO adsorption at 373 K on Pd(111) under all conditions employed, which is the most important point to be stressed about Fig. 10. The observation of this ν(N–O) mode in Fig. 10 indi-

cates that NO is molecularly adsorbed on Pd(111) at 373 K, and this mode is directly comparable to the low frequency N–O mode observed in Fig. 8 for low coverage NO adsorption on Pd(111) at 100 K.

NO adsorption at 373 K on Pd(112) produces vibrational spectra as shown in Fig. 11. The observation of a 1535 cm^{-1} ν(N–O) mode in Fig. 11 (bottom spectrum) indicates that NO adsorption is molecular on Pd(112) at 373 K. As the NO exposure is raised, this mode shifts to 1550 cm^{-1}, and another ν(N–O) mode at 1655 cm^{-1} is resolved following exposure to 6.9×10^{14} NO/cm^2. At the highest NO exposures, a strong 1670 cm^{-1} ν(N–O) feature with a low frequency shoulder is observed (top spectrum) in Fig. 11. No other ν(N–O) vibrational modes are observed from NO/Pd(112) following adsorption at 373 K under any conditions employed.

It is clear by direct comparison of Fig. 9 to Fig. 11 that NO adsorption on Pd(112) initially proceeds via the same site-filling sequence for adsorption at either 100 or 373 K. In addition, only one ν(N–O) band is observed following NO adsorption at 373 K
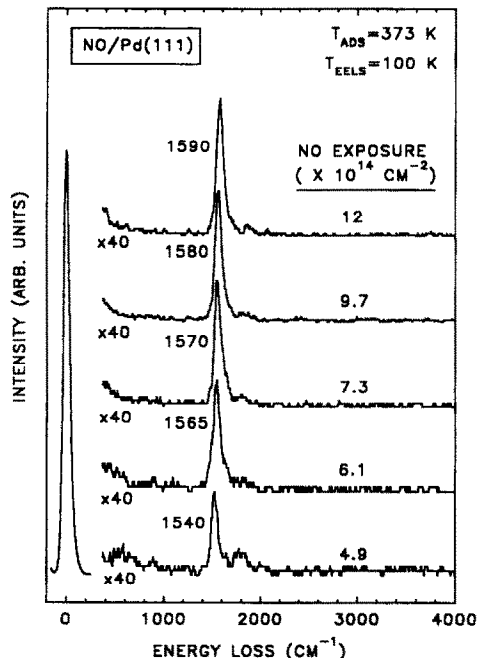

Fig. 11. High resolution electron energy loss spectra following adsorption of various amounts of NO on Pd(112) at 373 K. These spectra indicate that NO adsorption is molecular on Pd(112) under these conditions. By comparison with the low coverage spectra of Fig. 10 for Pd(111), the 1535 cm^{-1} ν(N–O) band observed in the bottom spectra is assigned to the vibrations of NO adsorbed at the (111) terrace sites of Pd(112). In addition, the 1655 cm^{-1} ν(N–O) mode observed here in the upper spectra, but not seen in Fig. 10 for Pd(111), is assigned to the vibrations of NO adsorbed at the (001) step sites of Pd(112).

on Pd(111) (Fig. 10), whereas under similar conditions two ν(N–O) modes are present in the vibrational spectra from NO/Pd(112) (Fig. 11). Direct comparison of these two figures indicates that the 1655 cm^{-1} feature in Fig. 11 results from ν(N–O) vibrations of NO adsorbed at the (001) step sites of Pd(112). Thus HREELS indicates that the low coverage adsorption ($100 \leqslant T_{ads} \leqslant 373$ K) of NO occurs preferentially on the (111) terraces of Pd(112), with both (111) terrace sites and (001) step sites becoming occupied at higher NO coverages.

3.2.3. Thermal behavior: NO / Pd(111) and NO / Pd(112)

The HREEL spectra of Fig. 12 illustrate the effect of heating an NO-saturated Pd(111) surface following NO exposure at 373 K. The decrease in fre-
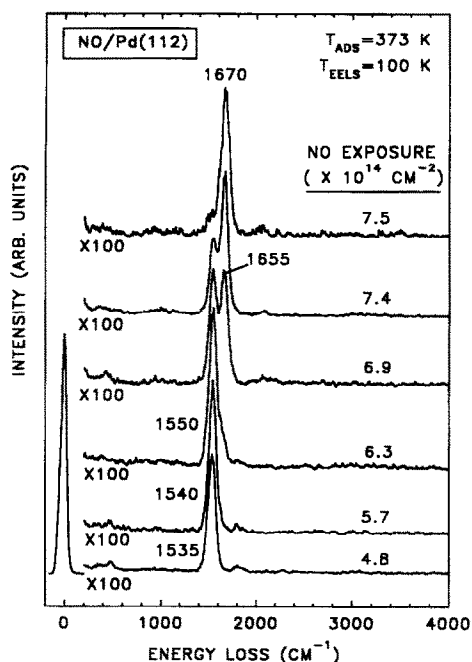

Fig. 10. High resolution electron energy loss spectra following adsorption of various amounts of NO on Pd(111) at 373 K. These spectra indicate that NO adsorption is molecular on Pd(111) under these conditions. Note that only one ν(N–O) mode is observed.

quency of the 1585 cm^{-1} ν(N–O) mode (bottom spectrum) in Fig. 12 with increasing annealing temperature is due to the removal of surface-bound NO via thermal desorption (i.e. the lower the NO coverage, the lower the ν(N–O) frequency). A similar shift of this ν(N–O) frequency with changing coverage is seen in Fig. 10.

The most significant change in the spectra of Fig. 12 is the appearance of a ν(Pd–O) mode at 525 cm^{-1} with a shoulder near 700 cm^{-1} upon heating above 490 K. This observation indicates that a small amount of NO dissociates upon heating above 490 K, leaving O(a) on the Pd(111) surface. This is consistent with the TPD results discussed in Section 3.1.1, where small relative yields of N$_2$ but no appreciable desorption of oxygen-containing species was observed from NO / Pd(111). This surface-bound O on Pd(111) diffuses into the Pd bulk at temperatures above 550 K, as evidenced by the disappear-

Fig. 13. High resolution electron energy loss spectra for various annealing temperatures following adsorption at 373 K of a high coverage ($\epsilon = 7.2 \times 10^{14}$ cm^{-2}) of NO on Pd(112). Heating to 460 K desorbs the step-site NO, producing a spectrum (second from the bottom) exhibiting a ν(N–O) mode at 1520 cm^{-1}, indicative of the presence of only terrace-bound NO. Heating above 490 K produces ν(Pd–O) modes at 500 cm^{-1} (surface O) and 1000 cm^{-1} (sub-surface O), indicating that NO thermal decomposition has deposited atomic oxygen at the Pd(112) surface.

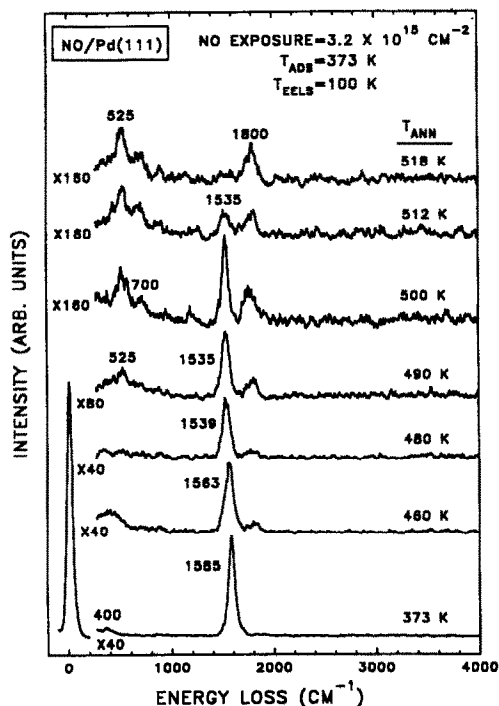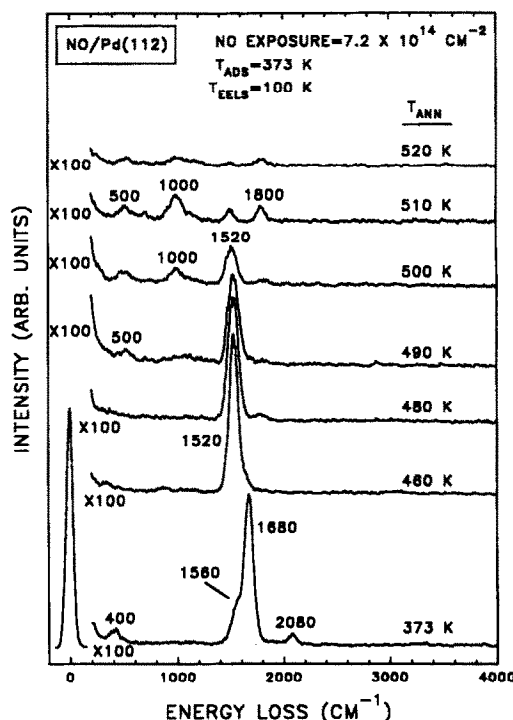Fig. 12. High resolution electron energy loss spectra for various annealing temperatures following NO adsorption at 373 K (exposure = $\epsilon = 3.2 \times 10^{15}$ cm^{-2}) on Pd(111). Heating above 490 K produces ν(Pd–O) modes at 525 and 700 cm^{-1}, indicating that NO thermal decomposition has deposited some atomic oxygen on the Pd(111) surface.

ance of the ν(Pd–O) modes in the HREEL spectra (not shown). It should be noted that a weak ν(Pd–NO) mode near 400 cm^{-1} in Fig. 12 (bottom spectrum) falls below HREELS detection limits after annealing to 480 K, and that this mode should not be confused with the 525 cm^{-1} ν(Pd–O) mode observed after heating to 490 K.

Fig. 13 shows the effect of heating on the vibrational spectra of a high coverage of NO adsorbed on Pd(112) at 373 K. The disappearance of the 1680 cm^{-1} ν(N–O) mode upon heating to 460 K (see the bottom two spectra of Fig. 13) is due to the thermal desorption of step-site NO, leaving only terrace-bound NO on the Pd(112) surface in the molecular form (see Fig. 11). As the surface is heated above

490 K, a ν(Pd–O) mode at 500 cm^{-1} is observed, indicative of NO dissociation. An additional oxygen-related vibrational feature is seen in Fig. 13 near 1000 cm^{-1}, also indicating that NO decomposes on Pd(112) upon heating. This 1000 cm^{-1} mode is believed to result from sub-surface O vibrational modes and will be discussed below.

Both surface-bound O and sub-surface O vibrational features from Pd(112) disappear in HREELS upon heating above 550 K (not shown), indicating that these species dissolve into the Pd bulk. It is noted that a weak ν(Pd–NO) mode observed near 400 cm^{-1} in Fig. 13 (bottom spectrum) falls below HREELS detection limits upon heating to 480 K, and that this mode should not be confused with the 500 cm^{-1} ν(Pd–O) band observed upon heating to 490 K. In addition, impurity CO in the presence of high coverage NO produces a weak vibrational loss at 2080 cm^{-1} in the bottom spectrum of Fig. 13, in addition to the usual ~ 1800 cm^{-1} mode seen in some of the other spectra.

The HREELS data of Fig. 14 are presented to show the effect of heating an NO/Pd(112) surface following a low NO exposure at 373 K. Here, only terrace sites are initially occupied by NO giving the singular 1525 cm^{-1} feature. It should be noted that the same features observed previously above 460 K in Fig. 13 are also evident in Fig. 14. Annealing above 490 K in Fig. 14 induces a slight decrease in frequency of the ~ 1525 cm^{-1} ν(N–O) mode and the appearance of bands associated with surface-bound O (520 cm^{-1}) and sub-surface O (990 cm^{-1}). Annealing above 550 K results in the diffusion of these oxygen species into the Pd bulk.

Comparison of the relative intensities between the ν(N–O) mode and the O-related modes in Fig. 13 (high NO coverage) with those of Fig. 14 (low NO coverage) for spectra acquired following 490–510 K annealing indicates that a larger relative amount of O is present in Fig. 14 than in Fig. 13. This is consistent with the TPD results of Fig. 7, where it was observed that the largest fractional NO decomposition on Pd(112) occurred for the lowest initial NO coverages upon heating.

3.2.4. O_2/Pd(112)

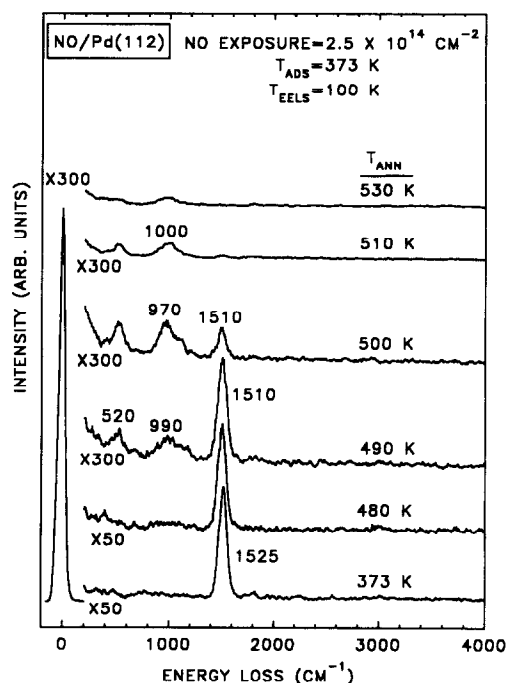Fig. 15 is presented as evidence that the 500 and 1000 cm^{-1} modes observed by HREELS from

Fig. 14. High resolution electron energy loss spectra for various annealing temperatures following adsorption at 373 K of a low coverage ($\epsilon = 2.5 \times 10^{14}$ cm^{-2}) of NO on Pd(112). The bottom spectrum, exhibiting a ν(N–O) mode at 1525 cm^{-1}, indicates the presence of only terrace-bound NO. Heating above 490 K produces ν(Pd–O) modes at 520 cm^{-1} (surface O) and 990 cm^{-1} (sub-surface O), indicating that NO thermal decomposition has deposited atomic oxygen at the Pd(112) surface.

Pd(112) following the thermal dissociation of NO are due to O-related vibrations. The left-hand side of Fig. 15 shows the thermal behavior of the vibrational spectra following 373 K adsorption of a low coverage of NO on Pd(112), whereas the right-hand side of Fig. 15 shows spectra acquired under similar conditions resulting from 373 K exposure of Pd(112) to 1.8×10^{14} O$_2$/cm^{-2}. Annealing NO/Pd(112) to 510 K produces vibrational modes at 520 and 1000 cm^{-1}, whereas annealing O$_2$/Pd(112) to 500 K produces a vibrational spectrum with 485 and 990 cm^{-1} vibrational features, as seen by comparing the bottom two spectra of Fig. 15. Also evident in Fig. 15 is the fact that annealing either system to above 550 K results in the decrease in intensity of these vibrational features to below HREELS detection limits. It should be noted that all of the spectra of Fig. 15 are plotted on the same scale.
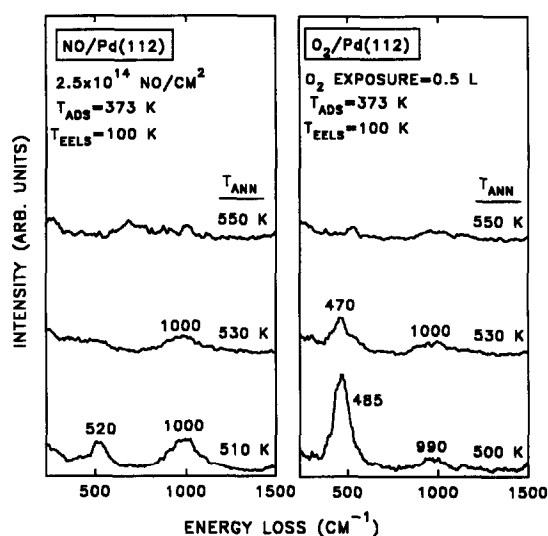
Fig. 15. High resolution electron energy loss spectra for various annealing temperatures following adsorption at 373 K of low coverages of NO ($\epsilon = 2.5 \times 10^{14}$ cm^{-2}, left-hand side) and O$_2$ ($\epsilon = 0.5$ langmuir $= 1.8 \times 10^{14}$ cm^{-2}, right-hand side) on Pd(112). The vibrational modes of surface O (~ 500 cm^{-1}) and sub-surface O (~ 1000 cm^{-1}) on Pd(112) are seen to exhibit similar thermal behavior in both systems. The disappearance of these bands above 550 K indicates the dissolution of O into the Pd bulk. The spectra are all plotted on the same scale.

These HREELS results, showing two vibrational bands which exhibit similar frequencies and thermal behavior on Pd(112) exposed to either NO or O$_2$ under similar conditions, indicate that these ~ 500 and ~ 1000 cm^{-1} modes are due to Pd–O vibrations. It is noteworthy that only ~ 500 cm^{-1}, and no ~ 1000 cm^{-1} vibrational features were observed by HREELS following NO or O$_2$ thermal dissociation on Pd(111) under conditions similar to those present in Fig. 15. Thus it appears that the formation of sub-surface O(1000 cm^{-1} band) is favored on Pd(112) as compared to Pd(111).

The HREELS data of Fig. 16 serve to illustrate one important point; pre-adsorbed oxygen does not preferentially block either the terrace sites or the step sites on Pd(112) toward NO adsorption. It is clear in Fig. 16 that NO adsorption at 373 K on clean (left-hand side) or O-covered (right-hand side) Pd(112) results in similar ν(N–O) vibrational bands for roughly the same NO exposures.

3.3. Electron stimulated desorption ion angular distributions

All of the ESDIAD data presented here were measured in the same UHV chamber at 100 K following adsorption of ^{14}NO at 300 K on clean Pd(111) and Pd(112) surfaces. O$^+$ ions were the only detectable particles observed during ESD from adsorbed NO in this study, and details about the O$^+$ ion identification, the O$^+$ ion kinetic energy distributions, and the dependence of the O$^+$ ion yield on the incident electron energy are presented in the Appendix. The O$^+$ ESDIAD patterns are shown in both perspective views and contour plots, the latter being generated by eight equal separations extending from 25% to 95% of the maximum counts on each plot. The ESDIAD patterns are shown with angular coordinate axes (which are slightly non-linear), arranged so that the macroscopic surface normal ($\langle 111 \rangle$ for
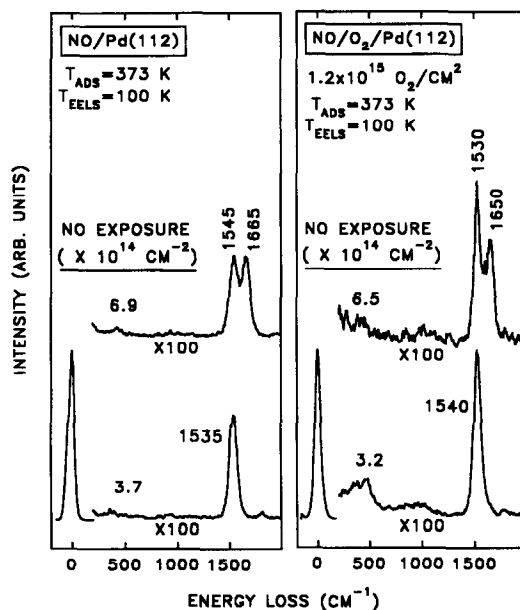
Fig. 16. High resolution electron energy loss spectra following 373 K adsorption of NO on clean (left-hand side) and O pre-covered (right-hand side) Pd(112). It is evident that essentially the same ν(N–O) modes are observed in both systems following nearly identical NO exposures. This result indicates that pre-adsorbed O does not preferentially block either the terrace sites or the step sites of Pd(112) toward NO adsorption under these conditions.

Pd(111) and ⟨112⟩ for Pd(112)) would project through the (0°, 0°) point of the patterns. The maximum polar angle of acceptance for positive ions (with respect to the surface normal) of the ESDIAD detector is roughly 48°.

3.3.1. NO / Pd(111)

Figs. 17 and 18 present O^+ ESDIAD patterns recorded with an incident electron energy of 800 eV from NO/Pd(111). The NO exposures employed in Figs. 17 and 18 were (a) 3.3, (b) 5.5, (c) 6.7, and (d) 8.9×10^{14} cm^{-2}. As can be seen in Figs. 17 and 18, the ESDIAD patterns from NO/Pd(111) consist of a single O^+ beam, oriented along the ⟨111⟩ surface normal direction. In addition, since all of the ESDIAD patterns of Fig. 17 are plotted on the same scale, it is evident that the O^+ signal increases with NO exposure. This is also seen in the contour plots of Fig. 18, where at low NO coverage (Fig. 18a) the

noise level is at or above 25% of the maximum counts in that pattern, whereas at high NO coverage (Fig. 18(d)) this is not the case.

The integrated O^+ ESDIAD signal calculated from data like those of Figs. 17 and 18 is shown in Fig. 19 versus NO exposure. It is evident from Fig. 19 that the O^+ yield from NO/Pd(111) rises monotonically as the NO exposure is increased, tending toward saturation at high NO exposures. The error bars of Fig. 19 (±5%) arise mainly from uncertainties due to the subtraction of a large X-ray background [6,7] followed by normalization.

Fig. 20 presents the half width at half-maximum (HWHM) of the same O^+ ESDIAD patterns from NO/Pd(111) analyzed for total O^+ yield in Fig. 19. It can be seen that within detection limits, the O^+ ESDIAD patterns remain centered about the ⟨111⟩ crystal azimuth and maintain a HWHM of ∼ 6° throughout the NO exposure range tested. This indi-

Fig. 17. Electron stimulated desorption ion angular distribution patterns (perspective views) of O^+ ions desorbed from NO/Pd(111) following various NO exposures at 300 K. The O^+ pattern is centered about the ⟨111⟩ surface normal direction (0°, 0°) at all coverages, indicating that the N–O bond remains normally oriented on Pd(111) under these conditions. The incident electron energy employed was 800 eV and the NO exposures, in units of 10^{14} cm^{-2}, were (a) 3.3, (b) 5.5, (c) 6.7, and (d) 8.9. The patterns are all plotted on the same scale, and the slightly non-linear axes (in deg) are provided for reference.

cates that under these conditions the NO molecules remain upright on Pd(111), with no evidence for tilted NO species being detected throughout the NO coverage range studied here. The error bars of Fig. 20 represent the absolute mean deviation in calculating the HWHM from the ESDIAD data.

3.3.2. NO / Pd(112)

The ESDIAD patterns of Figs. 21 and 22 were acquired with an incident electron energy of 1000 eV from NO/Pd(112). The crystal was positioned so that the step edge direction ($\langle\bar{1}10\rangle$ azimuth) is parallel to the left-hand border of each ESDIAD pattern (verified by LEED). In these figures, the $\langle112\rangle$ macroscopic crystal normal would intersect the (0°, 0°) coordinate, whereas the $\langle111\rangle$ terrace normal direction lies near (+19.5°, 0°). Angles less than 0° in the direction perpendicular to the step

edges correspond to the 'downstairs' direction, which is characteristic of NO adsorption on the step sites of Pd(112).

As can be seen in Figs. 21a and Fig. 22a, a low NO exposure (1.0×10^{14} cm^{-2}) on Pd(112) produces a single O$^+$ ESDIAD beam which is ejected near to the $\langle111\rangle$ terrace normal direction, *indicative of NO adsorption initially on terrace sites*. This single O$^+$ beam is observed up to NO exposures of 5.0×10^{14} cm^{-2}, as shown in Figs. 21b and 22b. However, at an exposure of 6.0×10^{14} cm^{-2} (Figs. 21c and 22c), NO/Pd(112) produces an ESDIAD pattern consisting of two O$^+$ beams, one oriented near the $\langle111\rangle$ terrace normal and the second in the 'downstairs' direction. This second O$^+$ beam increases in intensity at higher NO exposures (2.0×10^{15} cm^{-2}, Figs. 21d and 22d), indicating the increased occupation of Pd(112) step sites by NO
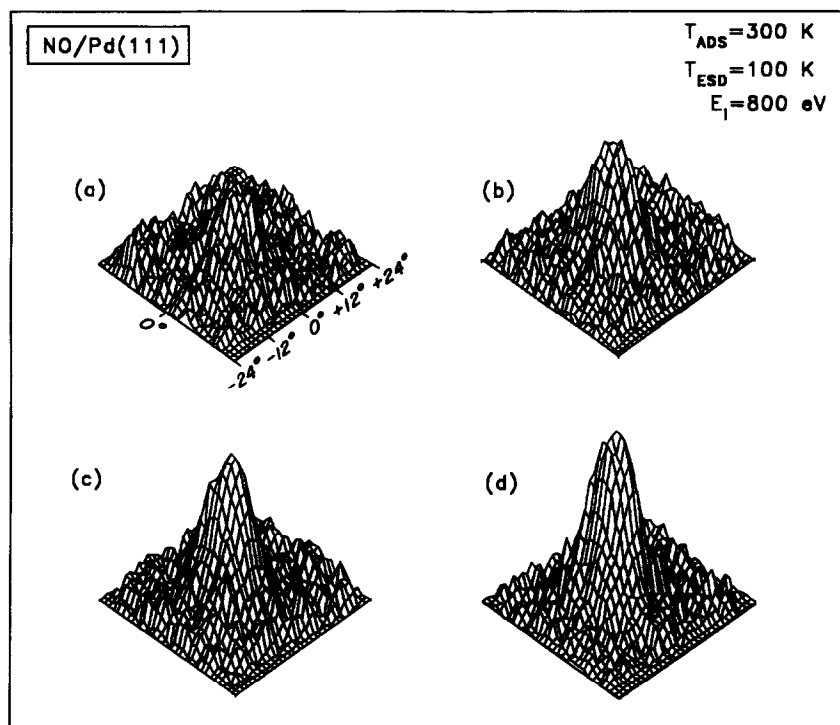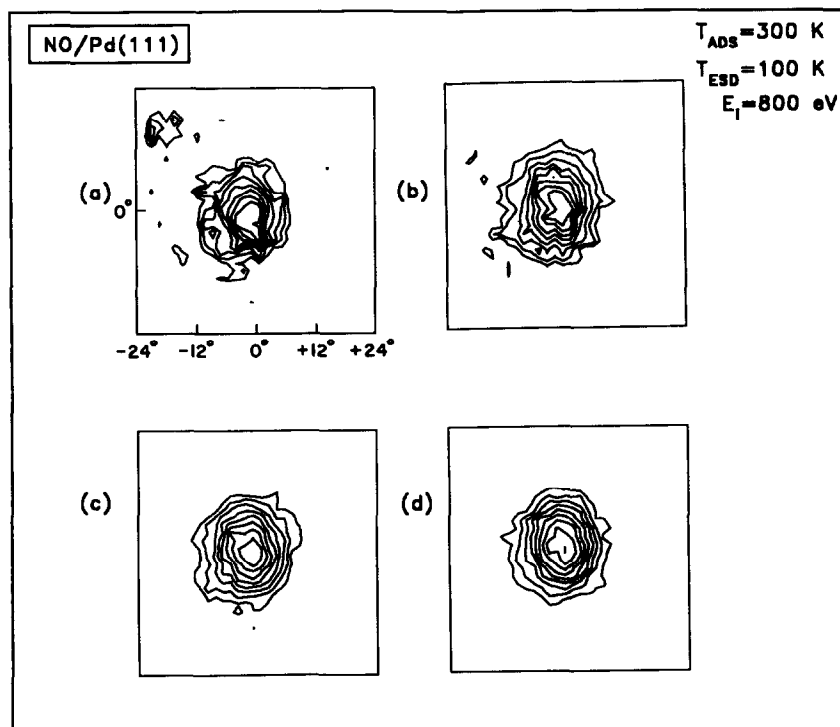

Fig. 18. Electron stimulated desorption ion angular distribution patterns (contour plots) of O$^+$ ions desorbed from NO/Pd(111) following various NO exposures at 300 K. The O$^+$ pattern is centered about the $\langle111\rangle$ surface normal direction (0°, 0°) at all coverages, indicating that the N–O bond remains normally oriented on Pd(111) under these conditions. The incident electron energy employed was 800 eV and the NO exposures, in units of 10^{14} cm^{-2}, were (a) 3.3, (b) 5.5, (c) 6.7, and (d) 8.9. The contour plots are generated by eight equal separations extending from 25% to 95% of the maximum counts in each plot, and the slightly non-linear axes (in deg) are provided for reference.
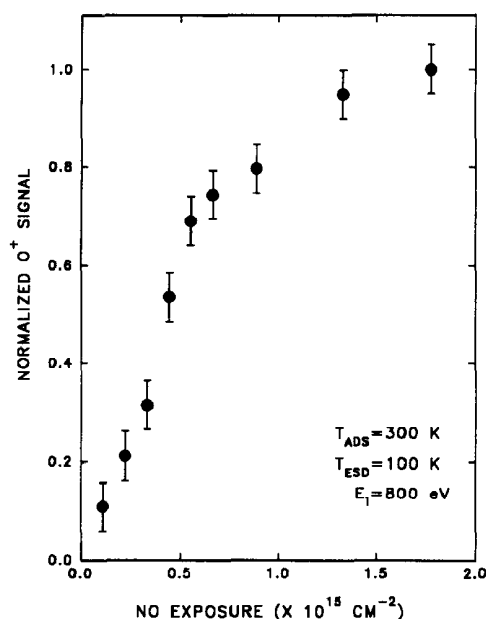
Fig. 19. Normalized yield of O^+ ions desorbed from NO/Pd(111) by electron stimulated desorption following adsorption at 300 K of various amounts of NO. The monotonic rise and saturation of the O^+ signal indicates the filling of the Pd(111) surface at 300 K by NO. The incident electron beam energy employed was 800 eV.

during later stages of adsorption. The ESDIAD results of Figs. 21 and 22 are entirely consistent with the HREELS data of Fig. 11, as will be discussed in detail below.

4. Discussion

The adsorption of NO on various single crystal Pd surfaces has been studied by a variety of techniques [11,14,16–29]. This study provides insight into the behavior of NO/Pd systems by detailed comparisons of data obtained from Pd(111) and Pd(112) surfaces under well-controlled conditions in the same laboratory. The properties of NO adsorbed on Pd(112) (composed of 3-atom-wide (111) terraces and monatomic (001) steps) has not been studied previously (to our knowledge) except in this laboratory [14,16]. In addition, this is believed to be the first detailed report of the ESD behavior of NO adsorbed on well-characterized Pd single crystal surfaces.

4.1. Thermal desorption and thermal decomposition of NO

The only thermal desorption species observed in this study from NO/Pd(111) and NO/Pd(112) were NO, N_2, and N_2O. The observation of only these three thermal desorption species, and not O_2 or NO_2, seems to be a consistent characteristic in a variety of NO/Pd systems [11,17,18,26,28]. These results imply that during heating, NO adsorbed on these Pd surfaces undergoes disproportionation reactions which favor the thermal desorption of N-containing species and preferentially deposit O at the Pd surfaces. This general conclusion, based on TPD results, will also be substantiated below by HREELS for the two specific cases considered in this study.

4.1.1. NO / Pd(111)

The TPD results of this study indicate that only minimal thermal decomposition of NO occurs on
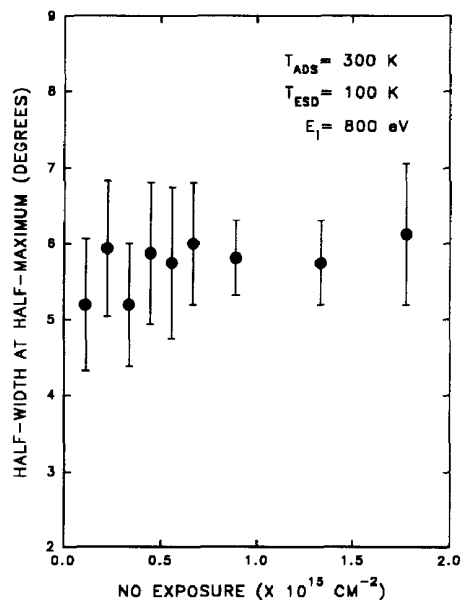
Fig. 20. Half width at half maximum (HWHM) of the O^+ ion angular distributions from NO/Pd(111) produced by electron stimulated desorption following 300 K adsorption of various amounts of NO. Within measurement limits, the HWHM maintains a value of ~ 6°, independent of the NO coverage. This result indicates that no evidence for tilted NO on Pd(111) is observed under these coverage conditions. The incident electron beam energy employed was 800 eV, and the data were acquired under field-free conditions.

Pd(111) during heating. This conclusion is based on the small relative yields of NO dissociation products, N_2 and N_2O, observed during TPD, and is consistent with previous conclusions about the thermal behavior of NO/Pd(111) [14,17,21,23,24]. It is likely that the low yield of NO decomposition products originates from defect sites on the Pd(111) single crystal used in this work. With this knowledge, it is reasonable to neglect the minority reaction channel (NO thermal decomposition) and to analyze the TPD spectra from NO/Pd(111) (Fig. 1) in detail in order to extract the kinetic parameters of NO thermal desorption.

The results of the application of TTPD analysis [15] to the TPD spectra of Fig. 1 appear in Figs. 2 and 3. The most obvious feature seen by comparison of Figs. 2 and 3 is that both kinetic parameters vary with NO exposure in the same manner. This 'compensation effect' has been observed in many adsorbate/substrate systems where lateral interactions between adsorbed particles play an important role [30–33]. Thus the decrease in E_{act} with increased NO exposure in Fig. 2 is interpreted as resulting from repulsive NO–NO interactions, which increase in strength as the average NO–NO distance decreases.

The second striking feature of Figs. 2 and 3 is that in the limit of zero coverage, the values of $E_{act} = E_{act}^0 \approx 180$ kJ/mol and the pre-exponential factor $\sim 10^{17}$ s^{-1} differ significantly from those usually found from a Redhead first-order desorption kinetic analysis [34]. However, the Redhead analysis assumes that no interactional effects occur between

Fig. 21. Electron stimulated desorption ion angular distribution patterns (perspective views) of O^+ ions desorbed from NO/Pd(112) following various 300 K NO exposures. All of the patterns contain an O^+ beam near the $\langle 111 \rangle$ terrace normal direction (+19.5°, 0°), resulting from NO adsorbed on the (111) terraces of Pd(112). A second O^+ beam, in the 'downstairs' direction (−16°, 0°) is observed *only at higher NO coverages*, and results from NO adsorbed on the (001) steps of Pd(112). The incident electron energy employed was 1000 eV and the NO exposures, in units of 10^{14} cm^{-2}, were (a) 1.0, (b) 5.0, (c) 6.0, and (d) 20. The patterns are all plotted on the same scale, and the slightly non-linear axes (in deg) are provided for reference. The macroscopic surface normal direction ($\langle 112 \rangle$) would intersect the patterns at (0°, 0°), and the step edges ($\langle \bar{1}10 \rangle$) run parallel to the left-hand border of each plot.

adsorbates (i.e., E_{act} = constant, independent of coverage).

It should be noted that no ordered LEED patterns from NO adsorbed on Pd(111) at 300 K were observed in this study, which is consistent with previous reports [17,22]. Thus the absolute NO surface coverage on Pd(111) following saturation of the ~ 510 K NO desorption state is difficult to determine, and estimates range from 1/4 ML [17] to 3/8 ML [22] to 0.43 ML [24].

The only detailed data available on coverage-dependent measurements of E_{act}, for NO desorption from a Pd surface with a structure similar to those studied here, were presented by Schmick and Wassmuth [18]. Those authors studied NO adsorption on a stepped Pd(111) crystal, cut at a 3° angle with re-

spect to the (111) face and exhibiting average (111) terrace widths of 16 atomic rows [18]. TPD spectra (dT/dt = 10.0 K/s) indicated the thermal desorption of NO and N_2O near 500 K, and two N_2 desorption maxima near 500 and 625 K [18]. The yield from the high temperature N_2 desorption state became saturated at low NO exposures, and no mention of the use of isotopic NO to verify these results was made [18]. Pre-exposure of the stepped surface to 0.4 langmuir of O_2 was found to completely eliminate the thermal dissociation of NO on this surface, presumably by blocking of the step sites by O(a) [18].

The TPD spectra (T_{ads} = 350 K) presented by Schmick and Wassmuth of NO from the stepped Pd surface, which was passivated toward NO dissocia-
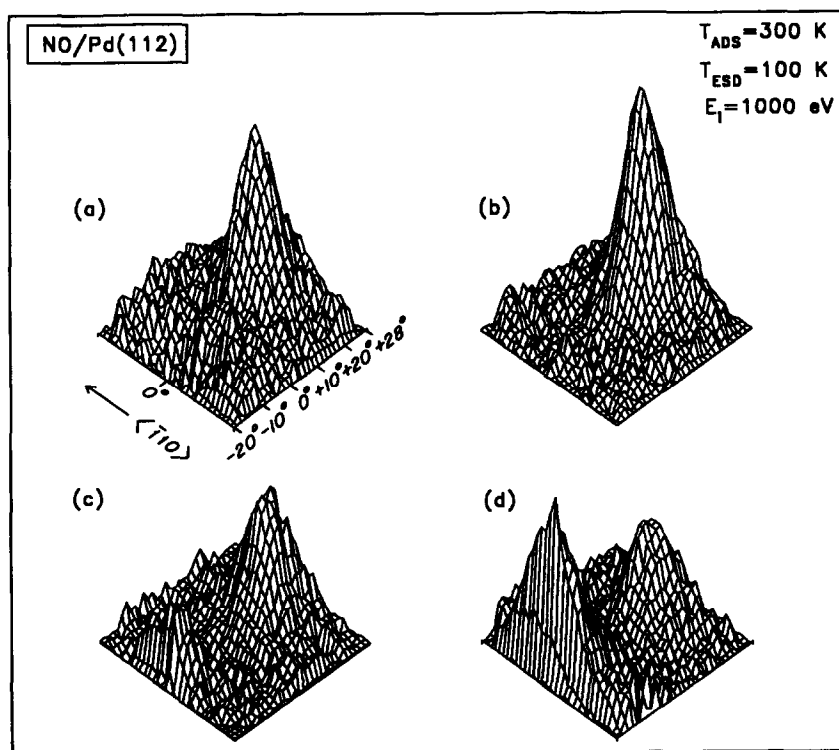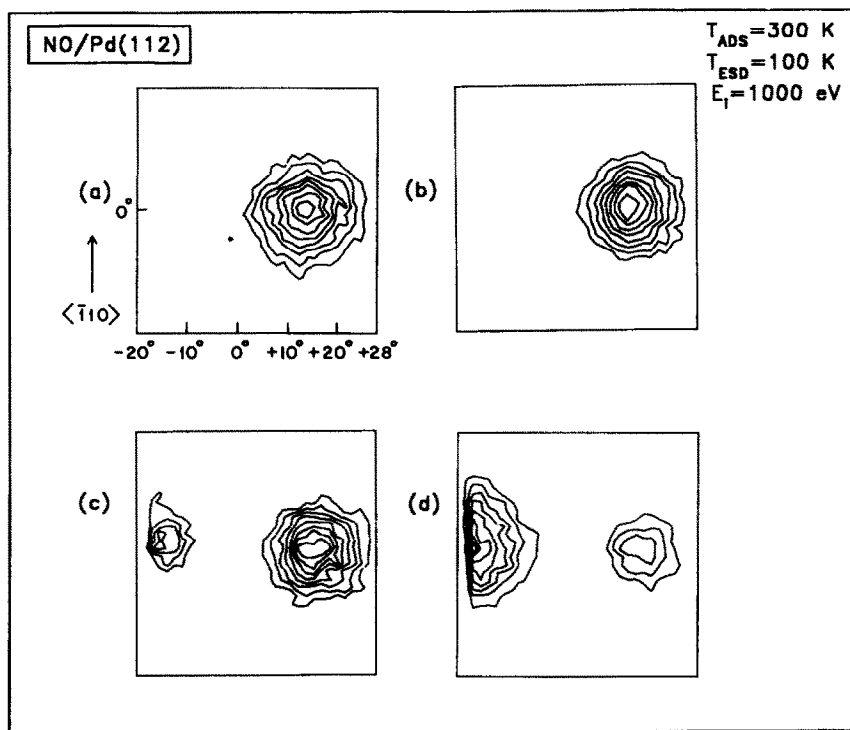

Fig. 22. Electron stimulated desorption ion angular distribution patterns (contour plots) of O^+ ions desorbed from NO/Pd(112) following various NO exposures at 300 K. All of the patterns contain an O^+ beam near the ⟨111⟩ terrace normal direction (+19.5°, 0°), resulting from NO adsorbed on the (111) terraces of Pd(112). A second O^- beam, in the 'downstairs' direction (−16°, 0°) is observed *only at higher NO coverages*, and results from NO adsorbed on the (001) steps of Pd(112). The incident electron energy employed was 1000 eV and the NO exposures, in units of 10^{14} cm^{-2}, were (a) 1.0, (b) 5.0, (c) 6.0, and (d) 20. The contour plots are generated by eight equal separations extending from 25% to 95% of the maximum counts in each plot, and the slightly non-linear axes (in deg) are provided for reference. The macroscopic surface normal direction (⟨112⟩) would intersect the patterns at (0°, 0°), and the step edges (⟨$\overline{1}$10⟩) run parallel to the left-hand border of each plot.

tion by pre-exposure to 0.75 langmuir of O_2 [18], exhibit the same general characteristics as those shown in Fig. 1. In addition, the data shown by Schmick and Wassmuth [18] for E_{act} versus NO coverage calculated via isothermic and isosteric desorption rates is also very similar in appearance to the data presented in Fig. 2. The only significant difference between the data of Fig. 2 and the qualitatively similar data of Schmick and Wassmuth [18] is the absolute magnitude of the energy scale for E_{act}. In Fig. 2, E_{act} for NO/Pd(111) varies from ~ 180 to ~ 90 kJ/mol, whereas Schmick and Wassmuth observed that E_{act} ranges from ~ 147 to ~ 71 kJ/mol for NO from the O-passivated (stepped) Pd(111) crystal [18].

The most reasonable explanation for these observed differences is that the presence of O on the surface studied by Schmick and Wassmuth [18] acts to lower the binding energy of NO at all coverages. Due to the 'compensation effect' [30–33], the absolute magnitude of the pre-exponential factor (v) for NO desorption presented here is also larger than reported by Schmick and Wassmuth [18], who indicate a value of 2.6×10^{14} s^{-1} at low NO coverage. A comparison of Figs. 2 and 3 indicates that in our experiments, when E_{act} has decreased to 147 kJ/mol at a finite NO coverage, our value for the pre-exponential factor is also $\sim 10^{14}$ s^{-1}. This could indicate that neighboring NO molecules act like O neighbors in reducing E_{act} and v, or that our kinetic measurements giving higher E_{act} and v at low coverage are carried out at lower coverages than those of Ref. [18].

The most important conclusions based on the TPD data of this section are that minimal thermal decomposition of NO occurs on Pd(111). In addition, strong repulsive interactions between the adsorbed NO molecules significantly lower the observed kinetic parameters for NO thermal desorption from Pd(111) as the NO surface coverage is increased.

4.1.2. NO / Pd(112)

The thermal desorption results from NO/Pd(112) shown in Figs. 4–6 indicate that NO undergoes partial dissociation on Pd(112) upon heating. As can be seen by the eye, and verified by integration [14], the TPD yields of N_2 and N_2O (Figs. 5 and 6, respectively) from NO/Pd(112) do not saturate as

the NO exposure rises. This result indicates that the amount of NO which decomposes on Pd(112) upon heating is not limited by the (fixed) number of defect or step sites on the Pd(112) surface. Additionally, the relative yields observed in Fig. 7 for the thermal desorption products of NO dissociation (N_2 and N_2O) indicate that the greatest fraction of NO molecules decompose upon heating at the lowest NO exposures. Although the absolute yield of each species increases as the NO exposure rises [14], the relative yields fall to a constant ratio as the NO coverage is increased, as shown in Fig. 7.

These observations based on TPD data indicate that lateral interactions between the species present on the surface during heating play an important role in determining the rate of NO dissociation with respect to the rate of NO desorption. As was observed in Fig. 2, repulsive NO–NO interactions lower the NO binding energy on Pd(111) by roughly 50% over the same exposure range in which the relative yields of N_2 and N_2O from NO/Pd(112) fall sharply (Fig. 7). In addition, since NO undergoes significantly more thermal decomposition on Pd(112) than on Pd(111) upon heating [14], lateral interactions between different adsorbed particles (NO, O and N) should be more important on Pd(112). The complexity of systems exhibiting lateral interactions between different adsorbates has been considered theoretically [30], but such treatments would need to be modified for application here due to the anisotropy presented by the stepped Pd(112) surface.

Results very similar to those of Fig. 7 were reported by Davies and Lambert in a study of the thermal behavior of NO adsorbed on a stepped Pd(331) surface [11]. The Pd(331) surface facetted after cleaning in UHV, but the (1×1)Pd(331) structure could be stabilized by the presence of O or S [11]. TPD spectra ($dT/dt = 20.0$ K/s) recorded after NO adsorption at room temperature on the (1×1)Pd(331) surface indicated NO, N_2 and N_2O thermal desorption near 550 K [11]. The relative yields of N_2 and N_2O presented by Davies and Lambert also decreased rapidly as the NO exposure was increased [11], exhibiting behavior qualitatively similar to the data shown here in Fig. 7.

The major trend observed in the data of Fig. 7 can be qualitatively explained by a model proposed by Davies and Lambert [11]. In this scenario, low cover-

ages of NO preferentially dissociate to N(a) and O(a) upon heating, due to the availability of many open Pd sites for accomodation of the products. Subsequent binary surface reactions then form N_2 and N_2O, which thermally desorb in relatively large quantities. In contrast, at high NO coverages few unoccupied Pd sites are available to bind the N and O products of NO decomposition. Therefore, NO desorption is favored over NO dissociation at high NO coverages, decreasing the relative yields of N_2 and N_2O that thermally desorb.

The most significant conclusions based on the TPD data of this section are that the presence of the (001) step sties on Pd(112) enhances the dissociation of NO upon heating, with respect to that observed from NO/Pd(111). In addition, the thermal decomposition of NO on Pd(112) is most important at low NO coverage, where only the (111) terrace sites are occupied by NO. Thus the criterion for NO thermal dissociation on Pd(112) is not step-site adsorption, but rather the presence of the empty step sites during heating, where surface diffusion, inter-particle lateral interactions, molecular decomposition and molecular desorption all occur simultaneously.

4.2. Vibrational properties of chemisorbed NO

The bonding of NO to metals (M) has historically been well-studied through investigation of metal nitrosyl complexes [35]. From such studies, it is generally concluded that NO bonds to metals through the nitrogen atom, which donates its lone pair electrons to the empty d orbitals of the metal to form a σ-type M–NO bond. In addition, back-donation of electron density from the metal d orbitals into the π* molecular orbitals of NO usually occurs. Here the extra 2π electron in NO dominates in determining the M–NO bond strength [36]. The relative efficiency of these competing exchanges of electron density between NO and the metal will determine the 'effective charge' that remains localized on the NO group after M–NO bond formation. Strong back-donation from the metal increases the NO^- character of the M–NO complex, and results in a weak N–O bond, exhibiting a low $\nu(N-O)$ stretching frequency, and a strong M–NO bond. Since the $\nu(N-O)$ frequency depends strongly on the 'effective charge' on the NO group, predictions of the bonding geometry of NO based

strictly on this vibrational frequency are questionable [35].

Nevertheless, many vibrational spectroscopic investigations of NO adsorbed on well-characterized metal surfaces have utilized the frequency of the $\nu(N-O)$ mode to predict the bonding geometry of NO at the surface (i.e. bridged, terminal, linear, bent, etc.). These assignments may be correct in some cases, but significant doubts have been recently raised as to the validity of assigning the adsorbate bonding geometry from vibrational spectra for the NO/ Ni(111) [37–39] and NO/Pt(111) [39] systems. Using photoelectron diffraction (PhD) [37], surface-extended X-ray absorption fine structure (SEXAFS) [38], and dynamical LEED [39] methods, quantitative bond lengths and geometries of NO adsorbed on Ni(111) [37–39] and Pt(111) [39] have been determined. These studies indicate that NO maintains a threefold coordinated hollow site bonding configuration on these two surfaces under conditions where the $\nu(N-O)$ frequency can vary from 1500 to 1800 cm^{-1}. However, these $\nu(N-O)$ frequencies of NO adsorbed on metal surfaces are usually interpreted by vibrational spectroscopists as indicating NO bound in twofold bridged and terminal sites, respectively [26].

With these considerations in mind, no discussion will be presented here concerning the assignment of a bonding geometry (bridged or terminal) of NO on Pd(111) or Pd(112). Instead, the coverage dependence and thermal behavior of the surface species yielding particular $\nu(N-O)$ stretching frequencies will be used comparatively. In fact, the conclusions drawn in this report do not depend on the bonding geometry of NO on its adsorption site, but only on the adsorption site identity (terrace or step). The adsorption site, as inferred here by direct comparison of the $\nu(N-O)$ modes observed by HREELS from NO/Pd(111) and NO/Pd(112), are also verified by a non-spectroscopic method (ESDIAD) in this report.

4.2.1. 100 K adsorption: NO / Pd(111) and NO / Pd(112)

Fig. 8 presents HREELS results recorded following 100 K exposure of Pd(111) to various amounts of NO. As can be seen in Fig. 8, low coverages of NO under these conditions produce a single $\nu(N-O)$ mode which increases in frequency from 1535 to

1600 cm^{-1} as the NO coverage rises, followed by the appearance of another distinct ν(N–O) vibrational feature at 1750 cm^{-1} at higher coverages. These observations from Fig. 8 are in agreement with the HREELS results of Bertolo and Jacobi [22], and Wickham et al. [24], and also with the infrared (IR) data of Chen and Goodman [25], all of which were recorded following 100 K adsorption of NO on Pd(111). In Fig. 8, spectra from many more NO coverages are presented than in Refs. [22] and [24]. The data of Fig. 8 will be used for direct comparison to HREELS data acquired from NO/Pd(112) under identical conditions.

The bottom half of Fig. 9 indicates that NO adsorbed on Pd(112) at 100 K at low coverage exhibits a ν(N–O) mode at 1522 cm^{-1} which increases in frequency (to 1540 cm^{-1}) as the NO coverage rises. The coverage dependence and frequency of this ~1540 cm^{-1} mode in Fig. 9 is similar to that observed in Fig. 8 from NO/Pd(111) under identical conditions. This direct comparison between NO on Pd(111) and Pd(112) is used to assign the ~1540 cm^{-1} vibrational feature of Fig. 9 to the ν(N–O) mode of NO adsorbed on the (111) terrace sites of Pd(112) at low coverage.

As the NO exposure is slowly increased in the bottom half of Fig. 9, another ν(N–O) mode near 1645 cm^{-1} is observed to increase in relative intensity and frequency. This ~1645 cm^{-1} band is not observed under any adsorption conditions from NO/Pd(111) (see Fig. 8 and Refs. [22,24,25]). In comparison, Pd(100) surfaces saturated by NO at 100 K and then annealed to 250 K (to remove weakly bound NO) exhibit a ~1678 cm^{-1} mode using HREELS [27] and ~1677 cm^{-1} mode using IR [25]. This ν(N–O) band shifts even lower in frequency in the IR spectra (to ~1655 cm^{-1}) as the NO surface coverage is depleted further by annealing to 350 K [25]. In addition, low (0.06 langmuir) NO exposure at 80 K on Pd(100) produces a ν(N–O) feature in HREELS at 1660 cm^{-1} [28]. With these results in mind, the ~1645 cm^{-1} mode observed in the bottom half of Fig. 9 is assigned as the ν(N–O) stretching frequency of NO adsorbed on the (001) step sites of Pd(112).

At the highest NO exposures on Pd(112) in Fig. 9, a ~1738 cm^{-1} ν(N–O) band with a small shoulder near 1638 cm^{-1} is observed. Under similar

conditions, high coverages of NO on Pd(111) produce HREELS bands near 1750 and 1600 cm^{-1} (see Fig. 8 and Refs. [22,24]). In addition, saturation of Pd(100) by NO at 80 K produces a broad ~1720 cm^{-1} feature in HREELS with a low frequency shoulder extending below 1500 cm^{-1} [28]. This same ν(N–O) band seen by HREELS [28] appears in IR spectra (following 100 K NO saturation of Pd(100)) as three modes near 1737, 1708, and 1695 cm^{-1} [25]. Upon consideration of these results, along with the possibility of through-bond and through-space NO–NO coupling and intensity sharing between ν(N–O) modes, the high exposure regime of Fig. 9 will simply be interpreted as resulting from the vibrations of a mixture of NO species adsorbed on both (111) terraces and (001) steps of Pd(112).

The most significant HREELS results presented in this section are that NO adsorption on Pd(111) and Pd(112) is molecular at 100 K. Additionally, it is concluded that NO adsorption on Pd(112) at 100 K occurs preferentially at (111) terrace sites following low NO exposures and that (001) step sites are only populated by higher NO exposures.

4.2.2. 373 K adsorption: NO /Pd(111) and NO /Pd(112)

The spectra presented in Fig. 10 resulted from HREELS measurements from NO/Pd(111) following various 373 K NO exposures. Only one ν(N–O) mode is observed in Fig. 10, exhibiting a frequency of 1540 cm^{-1} at low NO coverage which increases to 1590 cm^{-1} at high NO coverage. These results are in agreement with previous studies of NO/Pd(111) by HREELS [22,24] and IR [25]. By direct comparison, the ν(N–O) vibrational feature present in Fig. 10 is seen to be analogous to the low frequency ν(N–O) mode observed in Fig. 8 following 100 K NO adsorption on Pd(111).

Low coverage adsorption of NO on Pd(112) at 373 K (bottom half of Fig. 11) produces vibrational spectra with only one ν(N–O) band at 1535 cm^{-1}, which shifts to 1550 cm^{-1} at higher NO exposures. By comparison with the data of Fig. 10, which was acquired from NO/Pd(111) under identical conditions, the low frequency mode observed in the bottom half of Fig. 11 is assigned to ν(N–O) vibrations of NO adsorbed on (111) terrace sites of the Pd(112) surface.

Another $\nu(N-O)$ mode, assigned to NO adsorbed on (001) step sites, appears in Fig. 11 at 1655 cm^{-1} following an NO exposure of 6.9×10^{14} cm^{-2}. This assignment to (001) step sites is based on comparison of Fig. 11 with Fig. 10, where no equivalent $\nu(N-O)$ mode is observed from NO/Pd(111) under identical conditions. In addition, essentially the same behavior as seen in Figs. 10 and 11 for $T_{ads} = 373$ K is observed in HREELS data following low coverage NO adsorption on Pd(111) and Pd(112) at 100 K (Figs. 8 and 9, respectively). Thus the same comparisons to previous NO/Pd(100) vibrational studies [25,27,28] presented in the discussion of Fig. 9 (Section 4.2.1) are adopted here, further substantiating the assignment of the 1655 cm^{-1} band in Fig. 11 to $\nu(N-O)$ modes of NO adsorbed on the (001) steps of Pd(112).

High NO exposures on Pd(112) at 373 K produce a broad 1670 cm^{-1} vibrational feature in the top spectra of Fig. 11, with a low frequency (~ 1550 cm^{-1}) shoulder. This broad $\nu(N-O)$ feature results from a mixture of NO species, adsorbed at both (111) terraces and (001) steps of the Pd(112) surface.

The important conclusions drawn from the HREELS data of this section are that adsorption of NO on Pd(111) and Pd(112) at 373 K is molecular. In addition, NO has been shown to preferentially adsorb at low coverages on the (111) terrace sites of Pd(112) at 373 K, and to occupy the (001) step sites of this surface only at higher NO coverages.

The HREELS observation that NO adsorbs on Pd(112) at both 100 and 373 K in the same site-filling sequence (terrace followed by step) indicates that terrace-NO contains a weaker N–O bond than step N–O. This interpretation is consistent with the fact that terrace-bound NO on Pd(112) exhibits a $\nu(N-O)$ frequency (1520–1550 cm^{-1}) which is lower than that associated with step-site NO (1641–1655 cm^{-1}). According to the general statements made in the prologue (Section 4.2), a lower $\nu(N-O)$ frequency implies a weaker N–O bond. Thus the molecular adsorption of NO on Pd(112) follows a self-consistent yet counter-intuitive site-filling sequence.

4.2.3. Thermal dissociation: NO / Pd(111) and NO / Pd(112)

The HREELS data of Fig. 12 were recorded following a large NO exposure on Pd(111) at 373 K

and subsequent stepwise annealing. As the annealing temperature in Fig. 12 increases, the frequency of the $\nu(N-O)$ mode decreases from 1585 to 1535 cm^{-1}, indicative of the lowering of the NO surface coverage via thermal desorption.

The most important feature of Fig. 12 is the appearance of a $\nu(Pd-O)$ mode near 525 cm^{-1} with a shoulder near 700 cm^{-1} at an annealing temperature of 490 K. Banse and Koel observed a broad HREELS feature at 510 cm^{-1}, with shoulders near 425, 675, and 715 cm^{-1}, following the deposition of atomic oxygen on Pd(111) via the dissociative adsorption of NO$_2$ at 530 K [40]. Additionally, room-temperature O$_2$ adsorption on Pd(111) (to produce O/Pd(111)) yields a vibrational spectrum exhibiting a strong $\nu(Pd-O)$ mode at 485 cm^{-1} with weaker structure at 715 and 818 cm^{-1}, as observed by Imbihl and Demuth using HREELS [41].

Thus the weak 525 and 700 cm^{-1} vibrational features observed in Fig. 12 are interpreted as resulting from O(a), deposited on the Pd(111) surface by the decomposition of a small amount of NO during heating to 490 K. Annealing to 550 K was sufficient to remove these Pd–O features from the HREELS data, presumably due to the diffusion of this surface-bound O into the Pd bulk. These two conclusions are consistent with the TPD results discussed above, which indicated that small amounts of NO thermally dissociate on Pd(111) upon heating and deposit O on the surface, as evidenced by the observation of N$_2$ and N$_2$O, but not O$_2$ or NO$_2$ thermal desorption species. It is possible that the presence of a small percentage of defect sites on the Pd(111) surface is responsible for these minimal amounts of NO decomposition.

Fig. 13 presents the results of an HREELS investigation of the thermal behavior of a high coverage of NO adsorbed on Pd(112) at 373 K. Annealing to 460 K in Fig. 13 removes the NO adsorbed at the step sites of Pd(112) via thermal desorption, leaving only terrace-bound NO in the molecular form. *Note that no evidence is seen in the bottom two spectra of Fig. 13 that would indicate the dissociation of step-site NO on Pd(112) below 460 K.* It is seen that annealing to 490 K induces the decomposition of terrace-bound NO, evidenced by the appearance of a $\nu(Pd-O)$ feature of surface-bound O at 500 cm^{-1} in Fig. 13. In addition, the intensity of a 1000 cm^{-1}

mode is seen to rise, then fall, in Fig. 13 in the range $490 \leqslant T \leqslant 520$ K. This 1000 cm^{-1} band is assigned to Pd–O vibrations of O incorporated within the near-surface region of Pd(112), and will be discussed below. Both of these O-related vibrational features disappear following 550 K annealing, presumably due to absorption of the oxygen by the Pd bulk.

The HREELS data of Fig. 14 were recorded following low coverage adsorption of NO on Pd(112) at 373 K. In Fig. 14, exclusive NO adsorption on (111) terrace sites is indicated by the 1525 cm^{-1} ν(N–O) band (bottom spectrum). As the annealing temperature reaches 490 K, surface-bound O (520 cm^{-1}) and sub-surface O (990 cm^{-1}) vibrational modes are observed in Fig. 14, which increase and then decrease in relative intensity as the temperature rises. These results indicate that low coverage (ter-race-bound) NO partially dissociates on Pd(112) at 490 K, leaving O at the surface. Both of these O species dissolve into the Pd bulk following 550 K annealing, as evidenced by the disappearance of the Pd–O modes in the vibrational spectra.

One major conclusion of this section is that sur-face-bound O is formed as a product of NO dissocia-tion on both Pd(111) and Pd(112). This O(a) pro-duces a ν(Pd–O) mode in the frequency range 500–525 cm^{-1}, which appears at an annealing tempera-ture of 490 K and disappears upon annealing to 550 K, following the thermal dissociation of NO on both surfaces. The dissolution of O(a) into the Pd bulk is presumably responsible for this latter observation.

Another significant point stressed in this section is that sub-surface O (ν(Pd–O) $\approx$ 1000 cm^{-1}) is ob-served by HREELS only on Pd(112), and not on Pd(111), as a product of NO thermal decomposition. Similar behavior was observed in this study for dissociative O$_2$ adsorption; O/Pd(111) produces one vibrational mode ($\sim$ 500 cm^{-1}) whereas O/Pd(112) produces two modes ($\sim$ 500 and $\sim$ 1000 cm^{-1}). It is possible that the (001) steps on Pd(112) provide a low energy pathway which allows O to easily pene-trate into and to remain in the near-surface region below 550 K.

The final important observation in this section is based on comparison of the relative intensities of the ν(N–O) modes to those of the Pd–O modes in the spectra of Figs. 13 (high initial NO coverage) and 14 (low initial NO coverage) following annealing to 490–510 K. This comparison indicates that relatively more O is present in Fig. 14 than in Fig. 13 com-pared to NO, which indicates that a larger fraction of the NO decomposed at the lower initial NO cover-age. This observation is entirely consistent with the TPD results summarized in Fig. 7, where the relative yields of N$_2$ and N$_2$O were largest at the lowest NO exposures. This conclusion, drawn from both TPD and HREELS results, indicates that coverage-depen-dent inter-particle interactions play a major role in determining the fate of NO adsorbed on Pd(112) upon heating. Under high coverage conditions where NO–NO repulsions are significant, NO desorption is favored over NO decomposition on Pd(112).

4.2.4. O$_2$ / Pd(112)

The HREELS results obtained in this study fol-lowing the dissociative adsorption of O$_2$ on Pd(111) are consistent with previous HREELS studies of O/Pd(111) [40,41] and thus are not presented. How-ever, two results important to this paper concerning the presence of atomic oxygen on Pd(112) are dis-cussed in this section. These are (1) the formation of sub-surface O on Pd(112), and (2) the lack of prefer-ential site blocking (toward NO adsorption) by oxy-gen atoms on Pd(112).

First of all, the absorption of O into Pd is a well-known phenomenon [17,21,23,28,40–44], and presumably only a small energy barrier exists be-tween the adsorption of O on a Pd surface and the incorporation of O below the first Pd layer. How-ever, the presence of an O-related HREELS mode near 1000 cm^{-1} following NO or O$_2$ thermal de-composition on Pd(112), and not on Pd(111), is interesting. This result for Pd(112) is shown in Fig. 15, where low exposures of NO (left-hand side) and O$_2$ (right-hand side) at 373 K were performed, fol-lowed by stepwise annealing. Although the relative intensities of the O(a) mode ($\sim$ 500 cm^{-1}) and sub-surface O mode ($\sim$ 1000 cm^{-1}) differ following NO and O$_2$ dissociation, it is evident from Fig. 15 that both of these modes are O-related. In addition, both of these vibrational features exhibit the same thermal behavior whether produced from NO or O$_2$, falling below the HREELS noise level above an annealing temperature of 550 K in Fig. 15.

Sub-surface O formation has been proposed as a

possible explanation of anomalously high frequency O-related HREELS features observed from other transition metal surfaces [45,46]. Annealing Ni(111) [45] or Rh(110) [46] surfaces exposed to O_2 at low temperatures resulted in (presumably sub-surface O) HREELS bands near 970 and 984 cm^{-1}, respectively. In addition, heating NO/Ni(111) to 700 K, which liberated $N_2(g)$ and deposited O at the surface, produced an HREELS mode near 980 cm^{-1}, possibly indicative of the presence of sub-surface O [45].

These literature results [45,46], in conjunction with the data of Fig. 15, indicate that the ~1000 cm^{-1} HREELS mode observed in this study following NO thermal dissociation on Pd(112) (Figs. 13–15) is produced by sub-surface O species. The absence of such modes on Pd(111) (Fig. 12) implies that the (001) steps on the Pd(112) surface act as an efficient channel for O penetration into the near-surface region. Of course, more O is probably present on Pd(112) than on Pd(111) following NO thermal decomposition under similar conditions, because of the enhanced reactivity of Pd(112) toward dissociating NO. However, O deposition on Pd(111) via O_2 exposure, under conditions similar to that employed for the results shown in the right-hand side of Fig. 15, yielded no ~1000 cm^{-1} vibrational modes. Thus it seems that, independent of the amount of atomic oxygen available at the surfaces, Pd(112) forms both sub-surface and surface-bound O species, whereas only O(a) is formed on Pd(111).

Fig. 16 indicates that the pre-adsorption of atomic oxygen on Pd(112) does not preferentially block the step sites toward NO adsorption. As evident in Fig. 16, 373 K adsorption of NO on clean (right-hand side) and O pre-covered (left-hand side) Pd(112) produces essentially the same two ν(N–O) modes following virtually identical NO exposures. Low coverages of NO adsorb on the (111) terrace sites of Pd(112) (bottom two spectra) whereas both terraces and steps are occupied by NO at higher coverages (top two spectra) in Fig. 16. Therefore, the site-filling sequence of NO on Pd(112) observed in this study occurs regardless of the presence of O on the surface. Generally speaking, intuition would lead to the prediction that O will preferentially poison the step sites for NO adsorption, but this intuitive prediction is not supported by the data of Fig. 16. Possibly the adsorption of NO at the top of a step is not

influenced by the adsorption of O in the high coordination site at the bottom of a step.

4.3. Electron stimulated desorption ion angular distributions

The ESD behavior of NO adsorbed on W [47], Si [48,49], Ni [50–54], and Pt [55–58] surfaces has been studied previously; however NO/Pd systems have not been investigated by ESD methods to our knowledge [59]. Therefore, an appendix containing several experimental details about ESD from NO/Pd(111) is included at the end of this report. The results shown in the Appendix may be useful to workers in the ESD field, but do not affect any conclusions about the surface chemistry of NO/Pd drawn in the main body of this paper.

The ESDIAD technique is based on the measurement of the real-space distribution of particles desorbed from a surface during electron bombardment. From the 'initial-state' viewpoint, the observed ESDIAD patterns from these desorbing particles represent a statistical average over the instantaneous directions of the original chemical bonds ruptured by the ESD process [59]. In addition, the measured angular distributions may deviate from initial-state expectations due to the presence of anisotropic 'final-state' effects, which can act on the desorbing particles en-route to the detector [59–61]. However, the major conclusions presented in this section (based on initial-state concepts) are entirely consistent with the HREELS data discussed above, and thus final-state contributions to the ESDIAD patterns are considered to be of secondary importance.

In order to observe the angular distributions of O^+ ions from NO/Pd in a manner which should most directly reflect the N–O bond orientations at the surface, the ESDIAD patterns presented here were acquired under field-free conditions. Applying a positive bias to the crystal (with respect to the detector) is frequently used in many studies to enhance the positive ion counting rate, but this approach would modify the angular information required in this study. Because of the contribution of a large X-ray background at electron energies $\geqslant$ 800 eV, the signal-to-noise ratios of the ESDIAD patterns shown in this report are lower than usually seen in the literature [59].

4.3.1. NO / Pd(111)

All of the ESDIAD patterns recorded following NO adsorption at 300 K on Pd(111) consisted of a single O^+ beam centered about the $\langle 111 \rangle$ surface normal (see Figs. 17 and 18, where the NO exposure increases from (a)–(d)). In addition, the measured HWHM of these O^+ ESDIAD patterns does not strongly depend on the NO surface coverage (see Fig. 20). Although not shown here, essentially the same behavior was observed following 100 K NO adsorption on Pd(111), which yielded an O^+ beam normal to the surface with a HWHM of $\sim 6°$ in ESDIAD measurements. The major conclusions based on these observations are that NO remains upright on Pd(111) up to saturation coverages following adsorption in the temperature range 100–300 K, and that no evidence for tilted NO species on Pd(111) has been observed in this study. This interpretation is consistent with the angular-resolved ultra-violet photoelectron spectroscopy (ARUPS) study of Bertolo and Jacobi [22], where it was concluded that adsorbed NO remains basically perpendicular on Pd(111) at all coverages.

The data of Fig. 19 indicates that the total O^+ yield from NO/Pd(111) increases monotonically with NO exposure, tending to saturate at high NO coverage. In Fig. 19, the monotonic rise of the O^+ yield with NO exposure indicates that no ESDIAD evidence is found in this study for the presence of a minority of NO species (such as those adsorbed at random defect sites) which might possibly exhibit anomolously high ESD cross-sections [62,63]. The saturation behavior at high NO exposures is interpreted as resulting from the filling of the Pd(111) surface by NO adsorbed at 300 K, and no indication of strong intermolecular electronic quenching effects is seen in Fig. 19 [64].

4.3.2. NO / Pd(112)

Figs. 21 and 22 clearly indicate that as the NO exposure rises at 300 K (from (a)–(d) in these figures), the ESDIAD patterns from NO/Pd(112) consisting of a single O^+ beam at low coverages transform into two-beam patterns at larger NO exposures. The same sequence was observed at different adsorption temperatures (100 and 373 K). In all cases, the single O^+ beam from low coverages of

NO/Pd(112) is located near $(+14°, 0°)$ in the resulting ESDIAD patterns, close to the direction of the $\langle 111 \rangle$ terrace normal $(+19.5°, 0°)$. These results, combined with the HREELS data of Figs. 9 and 11, strongly indicate that NO preferentially adsorbs on the (111) terraces of Pd(112) at low coverages for adsorption temperatures in the 100–373 K range.

The appearance of a second O^+ beam in the ESDIAD patterns (at an NO exposure of 6.0×10^{14} cm^{-2} in Figs. 21c and 22c) oriented in the downstairs direction near $(-16°, 0°)$ is indicative of the presence of NO on the step sites of Pd(112). The relative intensity of the downstairs-directed beam increases as the NO coverage rises further (see Figs. 21d and 22d), indicating the increased occupation of step sites by NO. In these higher coverage ESDIAD patterns, the O^+ beam associated with terrace-bound NO appears near $(+16°, 0°)$, shifted slightly closer to the expected $\langle 111 \rangle$ direction than in the low coverage measurements.

Since the Pd(112) surface has a large step density, the local electron density distribution and the local electric field strength at the surface will be highly anisotropic [60,65–68]. The O^+ ions desorbed from NO/Pd(112) via ESD will experience this non-uniform electric field as they escape from the surface. This final-state effect is believed to be responsible for the deflection of the measured O^+ beam slightly away from the expected $\langle 111 \rangle$ direction for the terrace-bound NO. The possible presence of final-state effects in ESDIAD does not alter the major conclusion of this section, which is that NO adsorbs preferentially on the terrace sites of Pd(112) at low coverages in the temperature range 100–373 K, and only occupies the step sites at higher coverages.

4.3.3. Role of step sites in NO dissociation on Pd

The enhanced capability of stepped Pd(112) to dissociate chemisorbed NO is a key finding of this work. This enhanced dissociation occurs in response to the presence of step sites, *but not because of preferential NO occupation of the step sites*. There are a number of different ways to explain this unusual phenomenon and some are listed below while being schematically diagrammed in Fig. 23. It is not possible in this work to discriminate between the following three possibilities.
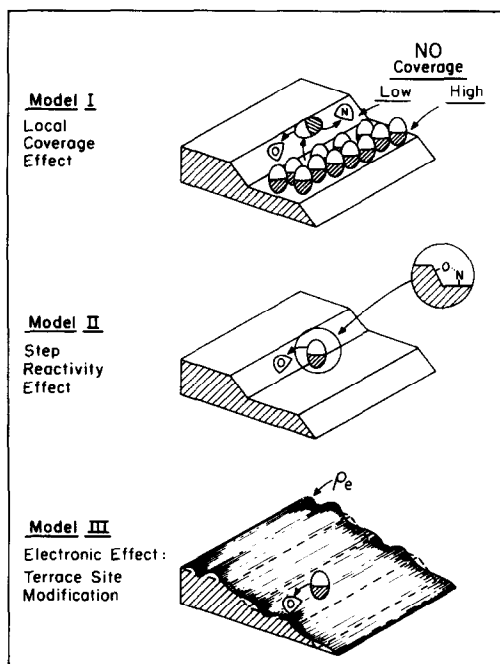
Fig. 23. Three possible mechanisms for preferential NO dissociation on Pd(112). These ideas are discussed in the text.

Model I. Local coverage effects

Our results suggest that the bonding of NO occurs preferentially on the terrace sites of Pd(112) due to stronger chemisorption on these sites. At the NO dissociation temperature near 500 K, the NO coverage will be high on the terrace sites and low on the step sites. In this model, then, a migrating NO molecule which happens to find itself on a step site will experience the presence of empty neighbor sites, promoting dissociation at low local coverages for steric reasons, in agreement with the model of Davies and Lambert [11].

Model II. Step reactivity effects

In this model, an NO molecule chemisorbed on a (111) terrace site may be able to sterically place the oxygen moiety favorably near a step Pd atom, promoting dissociation by strong bonding of both O and N to Pd atoms.

Model III. Electronic effect: terrace site modification

It is well known that charge density (ρ_e) variations due to step sites on metals extend into the terrace regions [65,68,69].

The electronic modification of the terrace sites due to this charge redistribution in the vicinity of the step sites may be responsible for the enhanced dissociation of NO on the terrace sites, and hence the increased activity of Pd(112) compared to Pd(111).

5. Conclusions

This report has presented a detailed comparison of NO adsorbed on Pd(111) and Pd(112) surfaces. The following results are found:

(1) NO adsorption on Pd(111) and Pd(112) is molecular in the temperature range 100–373 K.

(2) NO adsorbs upright on Pd(111) at all coverages, and no evidence for tilted NO species is observed.

(3) NO adsorbs at higher coverages in an inclined manner on Pd(112), with the N–O bond oriented in the downstairs direction.

(4) Upon heating, NO predominantly desorbs molecularly from Pd(111) near 500 K, with an activation energy and pre-exponential factor for desorption which strongly depend on the NO surface coverage. This indicates that coverage-dependent repulsive interactions between adsorbed NO molecules occur on Pd(111).

(5) Upon heating, relatively large amounts of N_2 and N_2O, in addition to NO, desorb from NO/Pd(112) in the temperature range 450–550 K. This indicates that the stepped Pd(112) surface is more active toward NO dissociation than the flat Pd(111) plane. However, preferential NO adsorption on the step sites of Pd(112) is not found, and cannot be responsible for the activity of the stepped surface toward NO decomposition.

(6) The fractional amount of NO decomposition upon heating is largest for the lowest NO coverages on Pd(112), irrespective of the fact that NO preferentially adsorbs on the (111) terrace sites of Pd(112) under these conditions.

(7) NO adsorption occurs preferentially on the (111) terraces of Pd(112) following adsorption in the temperature range 100–373 K, filling the (001) step sites only at higher coverages. This indicates that terrace-NO is more strongly bound to Pd(112) than step-NO. This observation is also an indication that NO is initially mobile on the surface, and is able to

seek out the strongest binding sites before being trapped.

(8) Vibrational modes of surface-bound O are observed following annealing of NO/Pd(111) to 490 K. This indicates that a small amount of NO dissociation occurs, possibly due to the presence of defect sites.

(9) Surface-bound O and sub-surface O vibrational modes are observed following annealing of NO/Pd(112) to 490 K, also indicating the thermal decomposition of NO. The presence of the (001) steps is believed to be responsible for the formation of sub-surface O on Pd(112), offering an efficient pathway for O incorporation within the near-surface region.

(10) Dissociative O_2 adsorption on Pd(111) and Pd(112) verified the exclusive formation of surface-bound O on Pd(111) and the presence of both surface and sub-surface O vibrational modes on Pd(112).

(11) Annealing to 550 K induces the diffusion of both surface-bound O (Pd(111); Pd(112)) and sub-surface O (Pd(112)) into the Pd bulk.

(12) The pre-adsorption of O on Pd(112) does not preferentially block either the step or the terrace sites toward NO adsorption.

Appendix

The experimental results presented in this Appendix provide details about the ESD behavior of NO/Pd that are not directly pertinent to the main conclusions of this paper. However, since this is the first detailed ESD study of NO/Pd systems to our knowledge [59], these results are included for completeness.

Fig. 24 shows that the only positive ion detected during ESD from NO/Pd in this study was O^+. Following adsorption of NO at 300 K (8.9×10^{14} cm^{-2}) on clean Pd(111), the surface was cooled to 100 K. The crystal was then positioned in front of the QMS (as for TPD, but with the QMS ionizer turned off) and was bombarded by electrons from an electron gun ($E_i = 900$ eV, $I = 8.8$ μA). The positive ions desorbed via ESD from the NO-covered Pd surface entered the QMS and were detected as shown in Fig. 24. A grid mounted in front of the QMS cage was biased negatively (with respect to the crystal) by
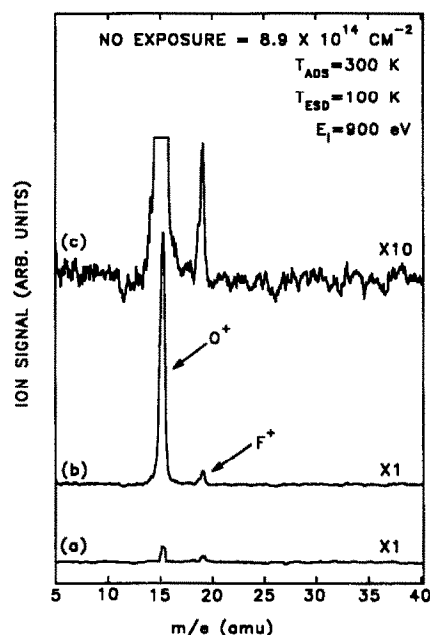

Fig. 24. Mass spectral identification of O^+ as the only detectable positive ion desorbed during electron stimulated desorption from NO/Pd(111). Following NO exposure ($\epsilon = 8.9 \times 10^{14}$ cm^{-2}) at 300 K, the Pd(111) surface was cooled to 100 K, where spectra (b) and (c) were recorded. The surface was then annealed to 1200 K to desorb NO, and cooled back to 100 K for acquisition of spectrum (a). The spurious F^+ signal originates from the electron gun itself, and the electron beam energy was 900 eV.

~ 3 V, in order to focus the positive ions into the QMS. It should be noted that a different electron gun than the one employed here for ion identification is used for ESDIAD data acquisition.

The mass spectra of Figs. 24b and 24c were recorded immediately after NO adsorption at 300 K and cooling of the crystal to 100 K. The crystal was then flash annealed to 1200 K to desorb the NO and was allowed to cool back to 100 K, where the data of Fig. 24a were recorded. As can be seen, O^+ is the major positive ion detected from the NO-covered Pd surface, and no evidence for N^+, NO^+, or O^{2+} is observed in Fig. 24.

The spurious F^+ signal seen in Fig. 24 was observed to decrease in intensity with an increase in the time that the electron gun was operated, independent of whether the gun was focused on the crystal surface during that time. This indicates that the F^+ signal arises from the electron gun itself, and not

from the Pd surface [70]. This effect can be seen even in Fig. 24, where ~ 30 min elapsed after acquisition of Fig. 24b and before the recording of Fig. 24a. Accordingly, the F^+ intensity in the latter spectrum is ~ 1/3 that of the former, due to the 'outgassing' of the electron gun during the ~ 30 min delay.

Fig. 25 shows the dependence of the O^+ ion intensity from NO/Pd(111) on the primary electron beam energy (uncorrected for work function differences). The clean Pd(111) surface was exposed to 7.3×10^{14} NO/cm^{-2} at 300 K, followed by cooling to 100 K. ESDIAD patterns were recorded for different E_i, with I held constant at 3.0 nA. In addition, a positive bias of 30 V was applied to the crystal to focus the O^+ ions into a sharp spot at the center of the resulting ESDIAD patterns. The maximum number of counts observed in this centrally compressed O^+ ESDIAD spot versus E_i is plotted in Fig. 25, where the + 30 V bias on the crystal has been added to the value of E_i in each case. The different data
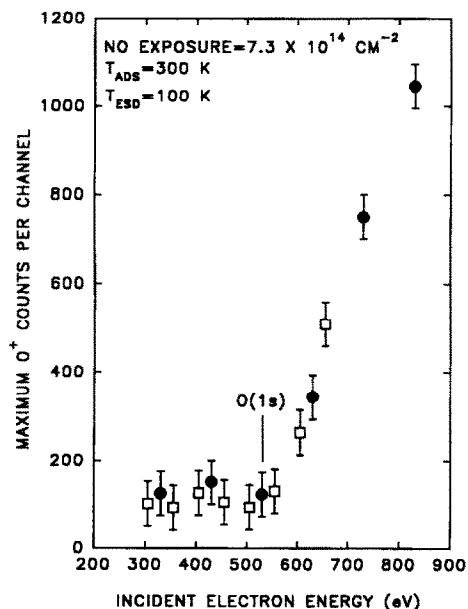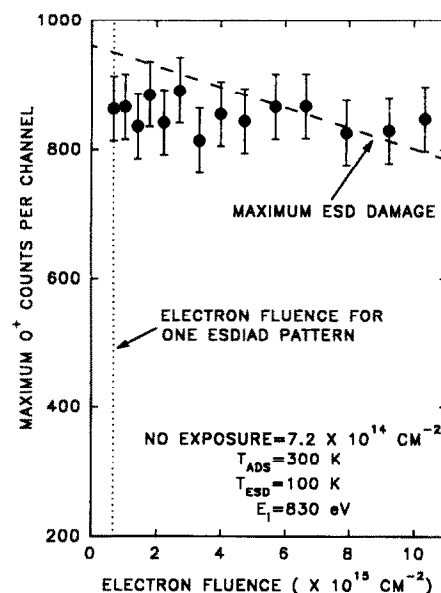

Fig. 26. The dependence of the O^+ intensity from NO/Pd(111) on the electron fluence employed for electron stimulated desorption measurements. It can be seen that within detection limits, essentially no change in the O^+ intensity occurs during the acquisition of one ESDIAD data set. An NO exposure of 7.2×10^{14} cm^{-2} was employed at 300 K, and the data were collected at an incident electron energy of 830 eV.

points (closed circles and open squares) resulted from two independent sets of measurements, indicating that the ±50 count error bars shown in Fig. 25 are reasonable.

As clearly seen in Fig. 25, a threshold for the enhancement of the O^+ ion intensity occurs ~ 30 eV higher than the O(1s) core level, the position of which is roughly indicated in Fig. 25. This observation is consistent with other studies of NO adsorbed on metal surfaces [51–53,55], where this energy threshold was attributed to O(1s) ionization combined with a single shake-off process.

In order to estimate the relative amount of ESD damage occurring during the acquisition of one ES-DIAD pattern, the data of Fig. 26 are presented. Here, NO (7.2×10^{14} cm^{-2}) was adsorbed on Pd(111) at 300 K, after which the crystal was cooled to 100 K. The electron gun energy and crystal current were fixed at 800 eV and 4.2 nA, respectively, and ESDIAD patterns were recorded as a function of time. A + 30 V bias was applied to the crystal (therefore $E_i = 830$ eV) and the maximum counts in

Fig. 25. Threshold measurement indicating that the O^+ yield from NO/Pd(111) is first detected at ~ 30 eV above the energy of the O(1s) core level. An NO exposure of 7.3×10^{14} cm^{-2} at 300 K was employed in two separate experiments, indicated by the filled circles and the open squares. No normalization of the two data sets or corrections for work function differences were performed.

the central O^+ beam (± 50 counts) are shown in Fig. 26 versus the calculated electron fluence.

It can be seen from Fig. 26 that, within detection limits, little change in the O^+ intensity occurs. The vertical dotted line indicates the maximum electron fluence that the surface is exposed to during the collection of one ESDIAD pattern (including electron beam focusing and other experimental adjustments). The dashed line indicates the worst-case scenario, in which the maximum amount of detectable ESD damage to adsorbed NO would occur viewing our data pessimistically. From the slope of this line, it is seen that during the time necessary for the collection of one ESDIAD pattern, the percentage change in the measured O^+ intensity and hence the ESD damage to chemisorbed NO is negligible ($< 1\%$).

Fig. 27 presents a retarding-grid measurement of the normal kinetic energy distribution of O^+ ions desorbed via ESD from NO/Pd(111). After NO exposure (1.6×10^{15} cm^{-2}) at 300 K, the crystal was cooled to 100 K. ESDIAD patterns were then

Fig. 28. Numerical derivative of a fourth-order polynomial fit to the data of Fig. 27. This curve, with a maximum near 3.9 V and an average HWHM of 5.1 V, represents a measure of the normal kinetic energy distribution of the O^+ ions desorbed from NO/Pd(111).
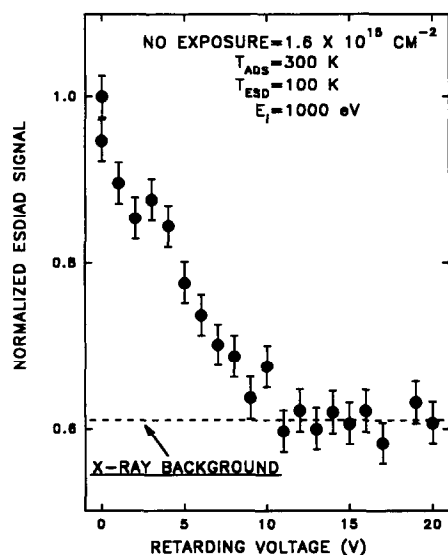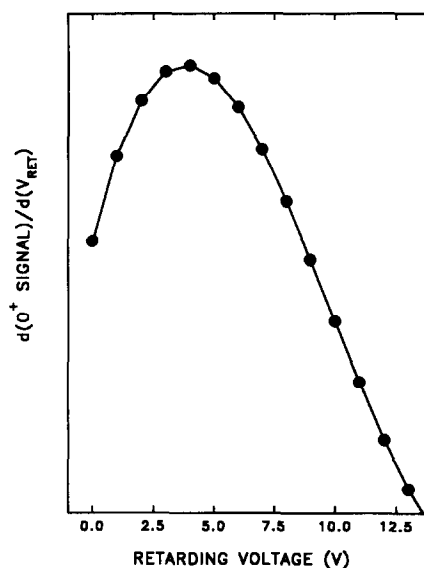

Fig. 27. The dependence of the signal observed during electron bombardment of NO/Pd(111) on the retarding voltage (positive with respect to the crystal) applied to the inner retarding grid of the ESDIAD analyzer. The O^+ ions from adsorbed NO are completely retarded at ~ 12 V, leaving only the X-ray background signal. An NO exposure of 1.6×10^{15} cm^{-2} at 300 K was employed, and the electron energy was 1000 eV. The abscissa has not been corrected for differences in work function.

collected ($E_i = 1000$ eV, $I = 3.0$ nA) with the crystal grounded, but with a positive 'retarding potential' (V_{ret}) placed on the third grid of the detection optics. This retarding voltage serves as the abscissa of Fig. 27, and is uncorrected for work function differences.

As evident in Fig. 27, the integrated ESDIAD signal decreases with an increase in V_{ret}, leveling off at ~ 12 V. The dashed line in Fig. 27 indicates the relative magnitude of the X-ray background (which is independent of V_{ret}) present in the ESDIAD patterns from NO/Pd before background subtraction. The measured X-ray background from a metal surface is known to increase with E_i [6], however so does the O^+ intensity from adsorbed NO (see Fig. 25). The presence of these competing effects explains the diminished signal quality of the O^+ ESDIAD patterns presented in the main body of this paper, compared to other ESDIAD studies where the X-ray background is smaller.

The data of Fig. 27 was fit to a fourth-order polynomial by a least-squares fitting routine. The derivative of the resulting function was calculated, and is plotted in Fig. 28 versus V_{ret}. It can be seen that the function in Fig. 28 is skewed, with a maxi-

mum near 3.9 V and an average HWHM of about 5.1 V. Although uncorrected for work function differences, the curve presented in Fig. 28 represents an estimate of the normal kinetic energy distribution of O^+ ions desorbed via ESD from NO/Pd(111).

Acknowledgement

References

[1] H.S. Taylor, Proc. R. Soc. London Ser. A 105 (1925) 108.
[2] See, for example: Chemistry in Two Dimensions: Surfaces, Ed. G.A. Somorjai (Cornell Univ. Press, Ithaca, NY, 1981).
[3] C.T. Campbell and S.M. Valone, J. Vac. Sci. Technol. A 3 (1985) 408.
[4] M.J. Bozack, L. Muehlhoff, J.N. Russell, Jr., W.J. Choyke and J.T. Yates, Jr., J. Vac. Sci. Technol. A 5 (1987) 1.
[5] A. Winkler and J.T. Yates, Jr., J. Vac. Sci. Technol. A 6 (1988) 2929.
[6] M.J. Dresser, M.D. Alvey and J.T. Yates, Jr., Surf. Sci. 169 (1986) 91; J. Vac. Sci. Technol. A 4 (1986) 1446.
[7] J.T. Yates, Jr., M.D. Alvey, K.W. Kolasinski and M.J. Dresser, Nucl. Instr. Methods B 27 (1987) 147.
[8] P.J. Chen, M.L. Colaianni and J.T. Yates, Jr., J. Vac. Sci. Technol. A 8 (1990) 764.
[9] R.G. Musket, W. McLean, C.A. Colmenares, D.M. Makowiecki and W.J. Siekhaus, Appl. Surf. Sci. 10 (1982) 143, and references therein.
[10] J.C. Tracy and P.W. Palmberg, J. Chem. Phys. 51 (1969) 4852.
[11] P.W. Davies and R.M. Lambert, Surf. Sci. 110 (1981) 227.
[12] J.C. Hamilton and J.M. Blakely, Surf. Sci. 91 (1980) 199.
[13] I. Ratajczykowa, J. Vac. Sci. Technol. A 1 (1983) 1512; Surf. Sci. 152/153 (1985) 627.
[14] R.D. Ramsier, Q. Gao, H. Neergaard Waltenburg and J.T. Yates, Jr., J. Chem. Phys. 100 (1994) 6837.
[15] J.B. Miller, H.R. Siddiqui, S.M. Gates, J.N. Russell, Jr., J.T. Yates, Jr., J.C. Tully and M.J. Cardillo, J. Chem. Phys. 87 (1987) 6725.
[16] Q. Gao, R.D. Ramsier, H. Neergaard Waltenburg and J.T. Yates, Jr., J. Am. Chem. Soc. 116 (1994) 3901.
[17] H. Conrad, G. Ertl, J. Küppers and E.E. Latta, Surf. Sci. 65 (1977) 235; 245.
[18] H.-D. Schmick and H.-W. Wassmuth, Surf. Sci. 123 (1982) 471.
[19] E. Miyazaki, I. Kojima, M. Orita, K. Sawa, N. Sanada, T. Miyahara and H. Kato, Surf. Sci. 176 (1986) L841.
[20] E. Miyazaki, I. Kojima, M. Orita, K. Sawa, N. Sanada, K. Edamoto, T. Miyahara and H. Kato, J. Electron Spectrosc. Relat. Phenom. 43 (1987) 139.
[21] S. Sugai, H. Watanabe, H. Miki, T. Kioka and K. Kawasaki, Vacuum 41 (1990) 90.
[22] M. Bertolo and K. Jacobi, Surf. Sci. 236 (1990) 143; 226 (1990) 207.
[23] S. Sugai, H. Watanabe, T. Kioka, H. Miki and K. Kawasaki, Surf. Sci. 259 (1991) 109.
[24] D.T. Wickham, B.A. Banse and B.E. Koel, Surf. Sci. 243 (1991) 83.
[25] X. Xu, P.J. Chen and D.W. Goodman, J. Phys. Chem., in press.
[26] R. Raval, M.A. Harrison, S. Haq and D.A. King, Surf. Sci. 294 (1993) 10.
[27] C. Nyberg and P. Uvdal, Surf. Sci. 204 (1988) 517; 211/212 (1989) 923.
[28] S.W. Jorgensen, N.D.S. Canning and R.J. Madix, Surf. Sci. 179 (1987) 322.
[29] J. Singh, W.K. Walter, A. Atrei and D.A. King, Chem. Phys. Lett. 185 (1991) 426.
[30] V.P. Zhdanov, Surf. Sci. 133 (1983) 469; 111 (1981) L662.
[31] J.W. Niemantsverdriet, K. Markert and K. Wandelt, Appl. Surf. Sci. 31 (1988) 211.
[32] J.W. Niemantsverdriet and K. Wandelt, J. Vac. Sci. Technol. A 6 (1988) 757.
[33] E.G. Seebauer, A.C.F. Kong and L.D. Schmidt, Surf. Sci. 193 (1988) 417.
[34] P.A. Redhead, Vacuum 12 (1962) 203.
[35] J.H. Enemark and R.D. Feltham, Coord. Chem. Rev. 13 (1974) 339;
G.B. Richter-Addo and P. Legzdins, Metal Nitrosyls (Oxford, New York, NY, 1992).
[36] M.E. Bartram, B.E. Koel and E.A. Carter, Surf. Sci. 219 (1989) 467.
[37] M.C. Asensio, D.P. Woodruff, A.W. Robinson, K.-M. Schindler, P. Gardner, D. Ricken, A.M. Bradshaw, J.C. Conesa and A.R. Gonzalez-Elipe, J. Vac. Sci. Technol. A 10 (1992) 2445; Chem. Phys. Lett. 192 (1992) 259.
[38] S. Aminpirooz, A. Schmalz, L. Becker and J. Haase, Phys. Rev. B 45 (1992) 6337.
[39] N. Materer, A. Barbieri, D. Gardin, U. Starke, J.D. Batteas, M.A. Van Hove and G.A. Somorjai, Phys. Rev. B 48 (1993) 2859.
[40] B.A. Banse and B.E. Koel, Surf. Sci. 232 (1990) 275.
[41] R. Imbihl and J.E. Demuth, Surf. Sci. 173 (1986) 395.
[42] M. Milun, P. Dervan, M. Vajic and K. Wandelt, Surf. Sci. 211/212 (1989) 887.
[43] J.-W. He, U. Memmert, K. Griffiths and P.R. Norton, J. Chem. Phys. 90 (1989) 5082.
[44] J.-W. He, U. Memmert and P.R. Norton, J. Chem. Phys. 90 (1989) 5088.
[45] See: H. Ibach and D.L. Mills, Electron Energy Loss Spectroscopy and Surface Vibrations (Academic Press, New York, NY, 1982) pp. 282-284, and references therein.

[46] D. Alfe, P. Rudolf, M. Kiskinova and R. Rosei, Chem. Phys. Lett. 211 (1993) 220.

[47] S. Sugai, H. Yoshikawa, H. Miki, T. Kioka and K. Kawasaki, Appl. Surf. Sci. 33/34 (1988) 301.

[48] M. Nishijima, K. Fujiwara and T. Murotani, J. Appl. Phys. 46 (1975) 3089.

[49] E.C. Ekwelundu and A. Ignatiev, Surf. Sci. 215 (1989) 91.

[50] F.P. Netzer and T.E. Madey, Surf. Sci. 110 (1981) 251.

[51] F. Bozso and Ph. Avouris, Chem. Phys. Lett. 125 (1986) 531.

[52] R. Jaeger, R. Treichler and J. Stohr, Surf. Sci. 117 (1982) 533.

[53] A. Takano and K. Ueda, Surf. Sci. 287/288 (1993) 25.

[54] A.R. Burns, Phys. Rev. Lett. 55 (1985) 525.

[55] U. Schwalke, H. Niehus and G. Comsa, in: Desorption Induced by Electronic Transitions (DIET II), Eds. W. Brenig and D. Menzel (Springer, Berlin, 1985) p. 98; Surf. Sci. 137 (1984) 23.

[56] A. Szabo, M.A. Henderson and J.T. Yates, Jr., J. Chem. Phys. 92 (1990) 2208.

[57] A.R. Burns, E.B. Stechel and D.R. Jennison, Surf. Sci. 280 (1993) 359.

[58] U. Heiz, J. Xu and J.T. Yates, Jr., J. Chem. Phys. 100 (1994) 3925;
U. Heiz, J. Xu, J.W. Gadzuk and J.T. Yates, Jr., J. Chem. Phys. 101 (1994) 4373.

[59] R.D. Ramsier and J.T. Yates, Jr., Surf. Sci. Rep. 12 (1991) 243, and references therein;
J.T. Yates, Jr., M.D. Alvey, M.J. Dresser, M.A. Henderson, M. Kiskinova, R.D. Ramsier and A. Szabo, Science 255 (1992) 1397.

[60] W.L. Clinton, M.A. Esrick and W.S. Sacks, Phys. Rev. B 31 (1985) 7540; 7550.

[61] Z. Miskovic, J. Vukanic and T.E. Madey, Surf. Sci. 141 (1984) 285; 169 (1986) 405.

[62] W. Jelend and D. Menzel, Surf. Sci. 40 (1973) 295; 42 (1974) 485.

[63] T.E. Madey, Surf. Sci. 94 (1980) 483.

[64] E.B. Stechel and M.L. Knotek, Surf. Sci. 167 (1986) 297;
F.P. Netzer and T.E. Madey, J. Chem. Phys. 76 (1982) 710.

[65] R. Smoluchowski, Phys. Rev. 60 (1941) 661.

[66] B. Krahl-Urban, H. Wagner and R. Butz, Surf. Sci. 93 (1980) 423.

[67] W.L. Clinton, M. Esrick, H. Ruf and W. Sacks, Phys. Rev. B 31 (1985) 722.

[68] J. Tersoff and L.M. Falicov, Phys. Rev. B 24 (1981) 754.

[69] Y. Hasegawa and Ph. Avouris, Phys. Rev. Lett. 71 (1993) 1071;
M.F. Crommie, C.P. Lutz and D.M. Eigler, Nature (London) 363 (1993) 524.

[70] J.T. Yates, Jr. and D.A. King, J. Vac. Sci. Technol. 9 (1972) 1256.